Are the C-band backscattering coefficient and interferometric coherence suitable substitutes of NDVI for the monitoring of the FAO-56 crop coefficient?

Nadia Ouaadi, Lionel Jarlan, Saïd Khabba, Michel LE PAGE, Adnane Chakir, Salah Er-Raki, Pierre-Louis Frison

Agricultural Water Management 282 (2023) 108276

Contents lists available at ScienceDirect

Agricultural Water Management

journal homepage: www.elsevier.com/locate/agwat

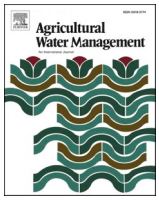

Are the C-band backscattering coefficient and interferometric coherence suitable substitutes of NDVI for the monitoring of the FAO-56 crop coefficient?

Nadia Ouaadi [a,b,c,*], Lionel Jarlan [a], Saïd Khabba [c,d], Michel Le Page [a], Adnane Chakir [c,e], Salah Er-Raki [d,f], Pierre-Louis Frison [e]

[a] CESBIO, University of Toulouse, IRD/CNRS/UPS/CNES, Toulouse, France
[b] GMME/SURFACE, Meteo-France/CNRM, Toulouse, France
[c] LMFE, Faculty of Sciences Semlalia, Cadi Ayyad University, Marrakech, Morocco
[d] CRSA, Mohammed VI Polytechnic University, Ben Guerir, Morocco
[e] LaSTIG, Gustave Eiffel University, Paris, France
[f] ProcEDE, Faculty of Sciences and Technologies, Cadi Ayyad University, Marrakech, Morocco

ARTICLE INFO

Handling Editor - Dr. Z. Xiying

Keywords:
Basal crop coefficient
Interferometric coherence
Polarization ratio
Evapotranspiration
Wheat crop

ABSTRACT

Rationalizing the use of agricultural water is a key issue in semi-arid areas that face more and more water shortages while food security is already threatened by the increasing population. The FAO-56 approach has been developed to estimate the crop water requirement. It relies on an accurate estimation of the "basal crop coefficient" $K_{cb\text{-}act}$ that has been shown to be closely related to NDVI. Nevertheless, optical data can be inoperant in case of persistent cloud cover. Within this context, the objective of this study is to assess the potentiality of the all-weather C-band Sentinel-1 radar observations available with 6-day revisit time at the field scale. To this end, the empirical relationships between $K_{cb\text{-}act}$, on one hand, and the interferometric coherence at VV (ρ_{VV}) and VH (ρ_{VH}) polarizations and the polarization ratio, on the other hand, were assessed on two wheat fields during two crop seasons and compared to the classical $K_{cb\text{-}act}$-NDVI method. It is demonstrated that while good statistical metrics are obviously obtained between $K_{cb\text{-}act}$ and NDVI derived from Sentinel-2 (R = 0.77/0.88 and RMSE = 0.14/0.15 for Field 1/Field 2), close results are highlighted with radar data. The best metrics are found with ρ_{VV}: R = 0.76 and 0.77 and RMSE = 0.18 and 0.28 for Field 1 and Field 2, respectively. Using the calibrated relationships on one season of Field 1, reasonable estimates of $ET_{c\text{-}act}$ was found on Field 1 (R = 0.70, RMSE = 0.75 mm/day and bias = −0.18 mm/days using $K_{cb\text{-}act}$-ρ_{VV}). By contrast, a significant overestimations is highlighted both with ρ_{VV} (bias = 0.73 mm/day) and NDVI (bias = 1.46 mm/day) over Field 2. Interestingly, the $K_{cb\text{-}act}$-ρ_{VV} relationship is more consistent in the estimation of $ET_{c\text{-}act}$ when changing from one plot to another. These outcomes open new perspectives for the estimation of $ET_{c\text{-}act}$ from radar data as a potential substitute of NDVI in case of persistent cloud cover.

1. Introduction

The global water demand is dominated by the irrigation sector that uses up to 90 % of available water in semi-arid catchments (Anapalli et al., 2020; Jarlan et al., 2015; Zhang et al., 2017). A rationale and sustainable use of the already scarce water resources in this region is becoming essential. Anticipation and efficient management of irrigation is also fundamental to ensure the global food security (IPCC, 2019; MedECC, 2020). This management is mainly based on the characterization of soil and vegetation water conditions that govern the use of water resources and this requires the estimation of crop water requirements which is represented by the evapotranspiration of the vegetation cover (ET).

The accurate estimation of ET constitutes the focus of several applications, starting from meteorology, since ET represents the process that transfers water from soil-plant to atmosphere (Allen et al., 2007; Gibelin, 2007; Norman et al., 1995; Soer, 1980), to agronomy, where ET defines the water requirements of the crop (Feng et al., 2019; Xiang

* Corresponding author at: CESBIO, University of Toulouse, IRD/CNRS/UPS/CNES, Toulouse, France.
E-mail address: nadia.ouaadi@univ-tlse3.fr (N. Ouaadi).

https://doi.org/10.1016/j.agwat.2023.108276
Received 6 October 2022; Received in revised form 8 March 2023; Accepted 14 March 2023
Available online 27 March 2023

et al., 2020; Yao et al., 2020). ET estimation can be done using in situ measurements such as the eddy covariance system and the lysimeters. Such techniques provide reliable estimates but they remain local and expensive to implement (Allen et al., 2011). Besides direct measurements, ET is computed using land surface models. Various types of models exist in the literature with a wide variety of theoretical background and required-input variables and can be divided into models based on resolving the energy balance and/or the water balance with different level of complexity (Ait Hssaine et al., 2021, 2018; Allen et al., 2011; Annandale et al., 1999; Bigeard et al., 2019; Courault et al., 2005; Diarra et al., 2017; Elfarkh et al., 2022; Jarlan et al., 2021; Subedi and Chávez, 2015; Zhang et al., 2016). The FAO-56 approach is a widely deployed model in the operational tools for irrigation management because it is easy to implement through a limited number of inputs (Allen et al., 1998). It was applied for several type of vegetation and has demonstrated accurate estimation over a wide range of climate and growth conditions around the world (Duchemin et al., 2006; Er-Raki et al., 2007; Pereira et al., 2021). It consists in multiplying the reference evapotranspiration (ET_0) of a well-irrigated grass derived from simple meteorological variables, by an empirical coefficient called the crop coefficient K_c that reflects the actual condition of the considered plant. Under this form, the determination of K_c is sufficient to obtain an estimate of the amount of water needed by the plant to preserve a good yield while avoiding waste of water (Pereira et al., 2021).

K_c varies throughout the agricultural season because of the phenological stages specific water demand and the changes of the aerodynamic and the surface resistances (Allen et al., 2011; Pereira et al., 2021). For annual crops, K_c is assumed to have a trapezoidal shape with four linear segments representing four main growing stages and subsequently three K_c values are required to obtain the whole growing season evolution. FAO-56 paper provides a large database of these values for a wide range of crops, and climates. However, previous work has demonstrated strong discrepancies between locally measured and the FAO tabulated values (Anapalli et al., 2020; Er-Raki et al., 2013; Howell et al., 1995; Irmak et al., 2013; López-Urrea et al., 2016; Pereira et al., 2021; Sánchez et al., 2015). Indeed, K_c is highly affected by several factors such as irrigation technique, crop cover fraction, agricultural practices, length of the growing season and local climate. K_c values and the duration of the different growth stages should thus be adjusted to reflect the actual condition of the considered crop (Allen et al., 1998; González-Dugo and Mateos; , 2008; Er-Raki et al., 2008; Pôças et al., 2020).

Because local calibration of K_c requires costly and time-consuming installations, remote sensing and, in particular, vegetation indices derived from optical data have been considered to exploit the high sensitivity of K_c to the vegetation cover fraction and to the Leaf Area Index (LAI) since the 1980s (Bausch and Neale, 1987; Diarra et al., 2017; Er-Raki et al., 2013; Wiegand et al., 1991). Several vegetation indices have been assessed (see Pôças et al., 2020 for a review) but the most widely used remains the NDVI (Duchemin et al., 2006; Er-Raki et al., 2013; French et al., 2020; Glenn et al., 2011; Hunsaker et al., 2005; Pereira et al., 2021; Pôças et al., 2020). Experience has shown that there is no general scientific framework that defines the nature of the relationship between K_c and NDVI as both linear (Bausch, 1993; Duchemin et al., 2006; Gontia and Tiwari, 2010; Hunsaker et al., 2003; Kamble et al., 2013) and non-linear relationships (Alam et al., 2018; Er-Raki et al., 2013; Pôças et al., 2020) have been established. Several operational tools based on K_c-NDVI relationships have already been developed so far: the Satellite Monitoring of IRrigation (SAMIR), a software package developed to estimate ET and spatialized irrigation water budget over large areas (Le Page et al., 2014; Simonneaux et al., 2009) that is part of the MODSPA modeling platform developed at CESBIO (http://osr-cesbio.ups-tlse.fr/Satirr/); the SatIrr tool for irrigation scheduling at the field scale. Pôças et al. (2020) also provided a number of websites for K_c mapping over several countries to support irrigation management.

While good estimates of evapotranspiration where obtained based on these K_c-NDVI relationships, optical data may be hampered by atmospheric conditions leading to images unavailability during long periods that could be problematic in cloudy regions or for winter crop monitoring. Indeed, the SWOT analysis (Strengths, Weaknesses, Opportunities and Threats) of the FAO-56 approach developed by Pôças et al. (2020) has clearly highlighted cloud cover as a threat to the application of the method when optical indices are used to derive K_c. Within this context, the main objective of this work is to assess the potentialities of all weather C-band radar data as a substitute to vegetation indices for K_c estimates from optical remote sensing.

Over the last decade, radar (or SAR for Synthetic Aperture Radar) data have become increasingly used for vegetation monitoring at the field scale mainly with the launch of the satellites Sentinel-1A in 2014 and 1B in 2016 as the main driver. Although C-band radar signals (wavelengths between 3.75 and 7.5 cm) provide a complex mix of ground and vegetation contributions, several authors have proposed variables derived from the signal intensity and phase that can be directly related to vegetation variables such as biomass, crop height, and cover fraction (Gherboudj et al., 2011; Greifeneder et al., 2018; Jacome et al., 2013; Li and Wang, 2018; Mattia et al., 2003; Ouaadi et al., 2020, 2021a; Srivastava et al., 2015; Veloso et al., 2017). In particular, while the radar backscattering coefficient (σ^0), a measure of the backscattered signal intensity, is sensitive to both soil and vegetation variables, the polarization ratio $PR = \sigma^0_{VH}/\sigma^0_{VV}$, where σ^0_{VH} and σ^0_{VV} stand for the backscattering coefficient at cross- (VH) and co- (VV) polarization respectively, was introduced to reduce the effects of soil and soil-vegetation interaction. Indeed, the PR has been shown to be more stable in time than the backscattering coefficient and follows the evolution of biomass during the agricultural season (Ouaadi et al., 2021a; Veloso et al., 2017). This ratio is recently used by Chintala et al. (2022) to estimate K_c over rice, sugarcane and vegetables. Their investigation was directed towards establishing a linear relationship between K_c and PR but poor correlations were obtained (correlations range from 0.01 to 0.31). Beside the signal intensity, the phase information acquired by radar sensors has also been shown to be related to the crop cycle through the interferometric coherence (ρ). ρ is a measure of the phase stability. It can be computed between: (i) two images taken by two antennas simultaneously from two different angles that overlook the same scene or; (ii) two images acquired by the same sensor over an orbit with exact repetition but taken at different times (Coltelli et al., 1996) such as for Sentinel-1 data (Frison and Lardeux, 2018). If the characteristics of the scatterers including both geometric (at the scale of the radar wavelength) and dielectric properties within the image does not change, ρ is equal to 1 while if the characteristics changes between two acquisitions a drastic drop of ρ can be observed. In particular for crops, vegetation growth and movement of the scatterers due to weather conditions, such as wind and rain, systematically causes ρ to drop (Frison et al., 2018). With the high temporal repetitivity provided by Sentinel-1 (6 days), research has been conducted to investigate and understand the behavior of ρ over annual crops based on the encouraging results of some early studies (Blaes and Defourny, 2003; Engdahl et al., 2001; Wegmuller and Werner, 1997). In particular, ρ has been used as complementary information to optical data for crop mapping and classification (Busquier et al., 2020; Mattia et al., 2015; Mestre-Quereda et al., 2020). In addition, strong relationships were recently highlighted between ρ and several vegetation variables, namely biomass, leaf area index, crop height and cover fraction by Ouaadi et al., (2020, 2021a).

Within this context, the objective of this work is to assess the potential of radar observations to estimate the FAO-56 crop coefficient as a surrogate to the classically used NDVI derived from optical data. To this end, two variables derived from Sentinel-1 data are investigated, namely PR and ρ at VV and VH polarizations. The study is carried out over 4 winter wheat seasons in Morocco. The following section presents the study site and the experimental data. Section 3 deals with the

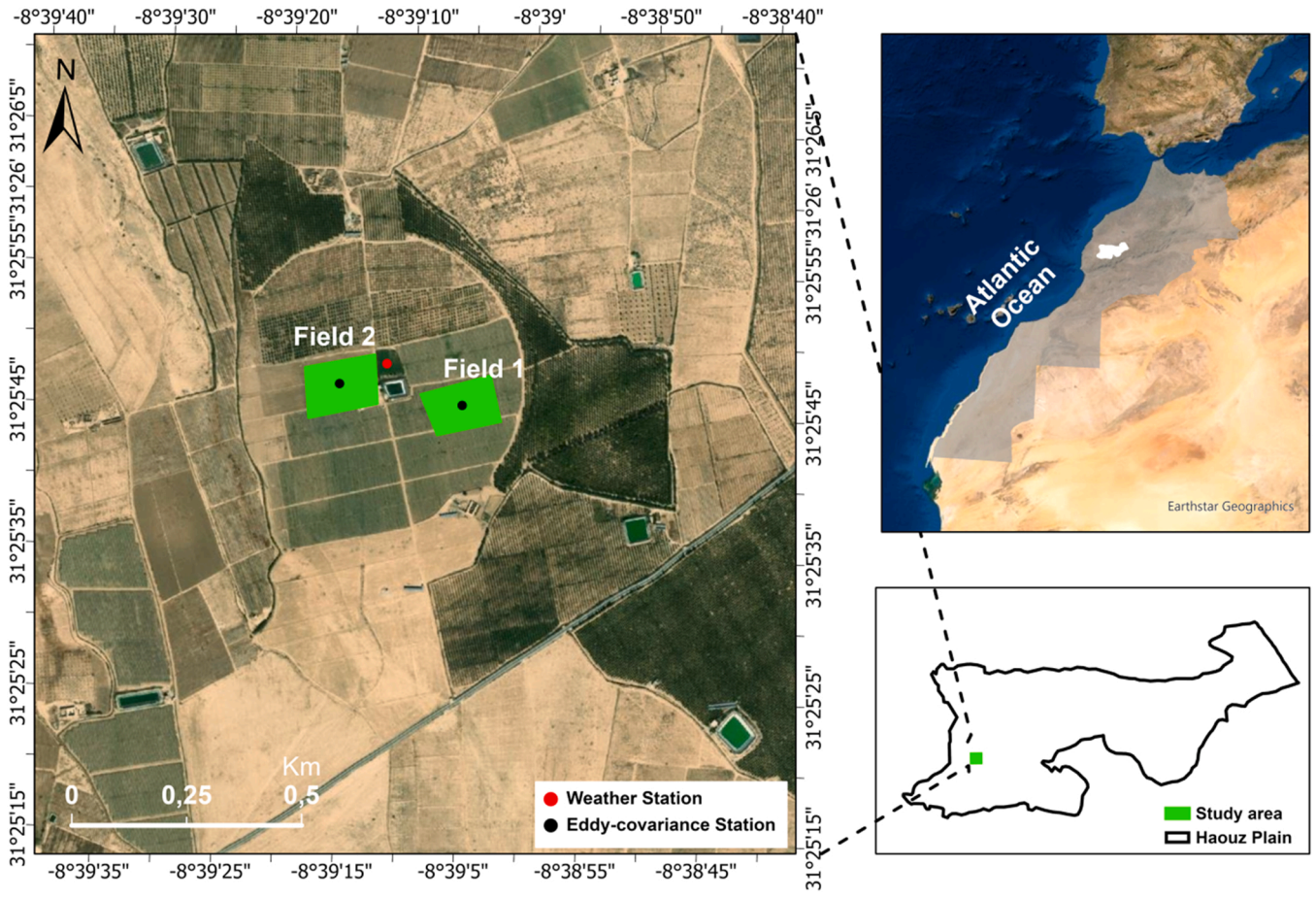

Fig. 1. Location of the monitored fields, weather and Eddy-covariance stations (left map) in the Haouz plain in central Morocco (right maps).

presentation of the results and it is organized as follows: (1) the time series of K_c derived from the eddy covariance system for the four seasons are presented; (2) the relationships between K_c and the radar variables are investigated and compared to K_c-NDVI relationship; (3) the calibration and validation of the K_c retrieved from the different variables are evaluated; (4) the ET derived from the estimated K_c over the four seasons is discussed. The last section is devoted to drawing conclusions.

2. Materials and methods

2.1. Study area description

The study area is located on a private farm in west-central Morocco in the Marrakech-Safi region, in one of the most important agricultural plains of the country named the Haouz plain (Fig. 1) characterized by a semi-arid climate. The air temperature is variable throughout the year, ranging from a hot summer with a daily average of about 35 °C in July-August to a cold winter with an average of 5 °C in January (Abourida et al., 2008). The average air humidity is about 50 % and the reference evapotranspiration ET_0 is about 1600 mm/year (Jarlan et al., 2015), which far exceeds the annual precipitation amount of 250 mm/year on average. Cereals, mainly wheat, represent the major portion of the irrigated and non-irrigated agricultural production of the plain. They are sown in winter when 85 % of the rainfall falls between October and April.

This study is conducted on two winter wheat fields monitored during two consecutive crop seasons 2016–2017 and 2017–2018. Fig. 1 illustrates the location of the fields in the Haouz plain. The soil texture is a mixture of 37.5 % clay and 32.5 % sand. The fields are drip irrigated and cover an area of 1.5 ha each, sown and harvested on the same dates. For the two monitored 2016–2017 and 2017–2018 seasons, the agricultural season starts with the sowing of wheat in late November (27/11/2016 and 25/11/2017) until the harvest on 16/05/2017 and 08/06/2018, respectively. The fields are sown by the Karim variety using an automatic seed drill with a distance of 15 cm between the sowing lines. In the 2016–2017 season, a stem density campaign conducted on March 28th resulted of an average of 416 and 504 stems/m^2 over Field 1 and Field 2, respectively. Unfortunately, the accurate value of the field density is not determined for the 2017–2018 season but the same tools were used for seeding resulting probably in seed densities of the same order of value. An estimation of the main crop growth stages starting dates reported during the field campaigns from visual inspection are provided in Table 1. The GDD (Growing degree days) corresponding to these dates is also provided in °C for the sake of information (calculated by accumulation of daily average temperatures). The fields are irrigated at a rate of

Table 1
Main growth stages starting dates of wheat crop during the 2016–2017 and 2017–2018 growing seasons.

	2016–2017		2017–2018	
	Date	GDD (°C)	Date	GDD (°C)
Emergence	05/12/2016	93[a]	08/12/2017	151[a]
Tillering	20/12/2016	174	28/12/2017	181
Extension	20/01/2017	–	25/01/2018	295
Heading	10/03/2017	620	18/03/2018	567
Senescence	07/04/2017	424	20/04/2018	469

[a] GDD computed between sowing and emergence dates. The GDD value between tillering and extension of the 2016–2017 season is not available due to the unavailability of air temperature data between 01/12/2016 and 08/01/2017.

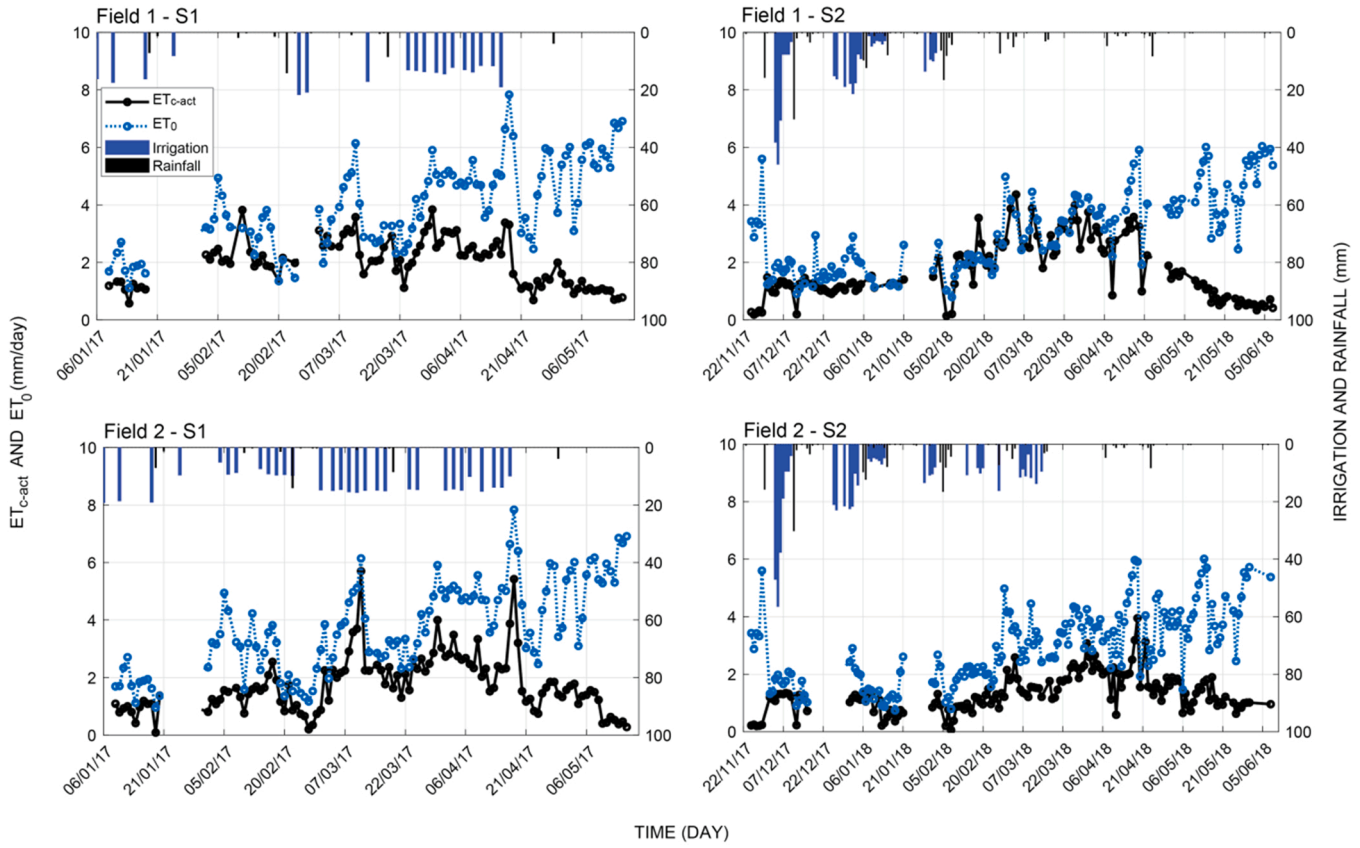

Fig. 2. Time series of the measured evapotranspiration ($ET_{c\text{-}act}$) and reference evapotranspiration (ET_0) over Field 1 and Field 2 and during the two agricultural seasons S1 (2016–2017) and S2 (2017–2018). The precipitation and irrigation amounts are also displayed.

12.5 mm per event and the irrigation scheduling and amounts are recorded (Ouaadi et al., 2021b).

2.2. *In situ measurements: weather and Eddy-covariance stations*

In the vicinity of the study sites, a weather station was installed over an irrigated alfalfa field (Fig. 1). The station allow a half-hourly measurements of precipitations and other meteorological variables used for estimating reference evapotranspiration (ET_0), namely solar radiation, wind speed and air temperature and relative humidity. Meteorological data were quality controlled to detect outliers following Boudhar (2009), Chaponnière et al. (2008) and Simonneaux et al. (2008).

To estimate continuous measurements of the actual crop evapotranspiration ($ET_{c\text{-}act}$), two similar eddy covariance stations (Campbell Scientific Ltd) are installed at 2.58 m high in the center of each field, as shown in Fig. 1. Each station is composed of a CSAT3–3D sonic anemometer and a KH2O-Krypton hygrometer, allowing the measurement of the three components of wind speed and the rapid fluctuations of atmospheric water vapor, respectively. The sampled raw data at 20 Hz rate are used to calculate the half-hourly sensible (H) and latent heat (LE) fluxes using the 'ECpack' software to apply all required corrections for planar fit correction, humidity and oxygen (KH20), frequency response for slow apparatus, and path length integration (Ait Hssaine et al., 2018; Rafi et al., 2019; Van Dijk et al., 2004). The measurements are representative of the field. To ensure that the flux contribution measured by the station is within the field, the calculation conducted for the study site conditions shows that 95 % of the flux information came from 50 × 32.5 m (long x wide) for a mean wind speed of 1.95 m/s and a wind direction of 58° (Rafi et al., 2019). Finally, the daily evapotranspiration (mm/day) is obtained by cumulating the 48 daily values of LE measurements excluding the negative values, and then converting from W/m^2 to mm/day. The stations are also equipped with Kipp and Zonen CNR radiometers to measure the net radiation Rn and two HFT3-L heat flux plates installed at 5 cm depth to measure the soil heat flux (G is computed by a simple average). Considering each field and season separately, the energy balance closure is acceptable: the correlation coefficient ranges between 0.70 and 0.81 while the slope of the linear regression between Rn-G and H+LE is between 0.47 and 0.56. These statistical metrics are within the range found in the literature in particular concerning the slope (see Elfarkh et al., 2020; Liu et al., 2011; Wilson et al., 2002 among others). The lack of closure of eddy covariance measurements was largely discussed in the literature and could be related to a combination of several factors (see (Allen et al., 2011)) including (i) the attenuation of turbulent signals at sufficiently low or high frequencies (Moore, 1986); (ii) the source area of the Rn and G sensors that measure the available energy is very small compared to that of the Eddy covariance system which can be changed rapidly depending on wind speed and direction and surface conditions; (iii) the energy storage either in the vegetation (Scott et al., 2003) or in the layer between surface and the heat flux plate measurements that is not considered in the energy balance closure (Meyers et al., 2004); (iv) the time shift between the irradiation and the turbulent fluxes that can reach up to 30 min (Foken et al., 2001, 2006). The modeling studies most commonly force the closing of the surface energy balance to correct the systematic under-estimation of turbulent fluxes measurements in particular because the energy balance is closed for the land surface models. The most extensively used method for this purpose is the Bowen ratio approach (Twine et al., 2000). This method is closing the energy balance by scaling H and LE so that the sum equals Rn-G. Considering the low value of the energy balance closure, both raw LE data (i.e. without correction) and LE values corrected by the Bowen ration approach are considered in this study. More details on this data base

including meteorological and eddy covariance data can be found in Ait Hssaine et al. (2018, 2020) and Rafi et al. (2019) and part of the data set has been made available to the scientific community (Ouaadi et al., 2021a).

Fig. 2 displays the time series of the raw measured $ET_{c\text{-}act}$ and computed ET_0 (see Section 2.3) over the two fields. For the sake of simplicity, the 2016–2017 season is designated by 'S1' and the 2017–2018 season by 'S2'. The difference between ET_0 and $ET_{c\text{-}act}$ is significant during the growing season characterizing the high climatic demand of the semi-arid region. ET_0 is higher in S1 than in S2 because of wetter conditions in the second season where the amount of rainfall recorded from sowing to harvest is 167 mm versus 70 mm during season S2 and season S1, respectively (Ouaadi et al., 2021a). The general trend is an increase during the agricultural season, with minimum values occurring in December and January around 2 mm/day. This period corresponds to the start of the season, ET_0 is higher than $ET_{c\text{-}act}$ because most of $ET_{c\text{-}act}$ comes from soil evaporation since canopy cover is very low (Allen et al., 1998), whereas ET_0 is the ET of a well-developed grass and will therefore use more water for transpiration (Araya et al., 2011). The $ET_{c\text{-}act}$ starts to increase with the development of the canopy with an average increase of 3 mm/day from the beginning of the season to full development. In addition to the higher seed density on Field 2 compared to Field 1, irrigation was stopped from 27/02/2017 to 14/03/2017 on Field 1 which led to a lower $ET_{c\text{-}act}$ of 2.5 mm/day on this field compared to Field 2. Moreover, $ET_{c\text{-}act}$ reached a maximum of 4.5 mm/day on Field 1 while the maximum on Field 2 is about 6 mm/day. The wetter 2017–2018 season contributed to the increase of the $ET_{c\text{-}act}$ of Field 1 to reach higher values than the first season and joined the ET_0 level in the mid-season stage. For Field 2, season S2 was affected by a particular growing condition (explained with more details in Ouaadi et al., 2021a). The presence of dense weed in the field as well as strong winds that laid down the high stems in April may be the reason for the low values observed of $ET_{c\text{-}act}$. $ET_{c\text{-}act}$ decreases obviously at the end of the season from the senescence phase onwards as the vegetation and the underlying soil dry out.

2.3. Actual single and basal crop coefficients

The reference evapotranspiration ET_0 is the evapotranspiration from a well-watered grass that totally cover the soil with a uniform height of 0.12 m, albedo of 0.23 and a surface resistance of 70 s/m. It is a climatic variable that account only for the evaporating power of the atmosphere. According to the FAO-56 guidelines, ET_0 is computed from the meteorological forcing using the Penman-Monteith equation:

$$ET_0 = \frac{0.408\Delta(R_n - G) + \gamma \frac{900}{T+273} u_2 (e_s - e_a)}{\Delta + \gamma(1 + 0.34u_2)} \quad (1)$$

Where R_n (MJ/m^2/day) is the net radiation at the crop surface and G (MJ/m^2/day) is the conductive flux in the soil. u_2 (m/s) is the wind speed at 2 m above the ground, T (°C) is the averaged air temperature at 2 m, γ (kPa/°C) is the psychrometric constant, e_s (kPa) and e_a (kPa) are the saturation and actual vapor pressures at 2 m, respectively. G is assumed to be equal to 0 for daily calculation while the other variables are computed using the daily meteorological forcing as in Allen et al. (1998).

The crop evapotranspiration ET_{c-act} is computed as introduced in the paper 56 of the FAO by Allen et al. (1998):

$$ET_{c-act} = K_{c-act} ET_0 \quad (2)$$

where $K_{c\text{-}act}$ is the crop coefficient that account for the soil evaporation, plant transpiration and the effect of water stress via three coefficients:

$$K_{c-act} = K_s K_{cb-act} + K_e \quad (3)$$

where K_s is the water stress coefficient, K_{cb-act} is the basal crop coefficient and K_e the evaporation coefficient.

This study focuses on the estimation of $K_{cb\text{-}act}$ and $ET_{c\text{-}act}$. To do so, the following steps are implemented:

i) The ratio of $ET_{c\text{-}act}$ measurements to the ET_0 (resulting in the crop coefficient $K_{c\text{-}act}$) has been filtered from high evaporation and water stressed data so that the remaining data correspond to $K_e \sim 0$ and $K_s \sim 1$ and therefore approximate the basal crop coefficient $K_{c\text{-}act} = K_{cb\text{-}act}$. The method is adapted from Duchemin et al. (2006). First, an initial cleaning of the database was performed by eliminating days corresponding to watering events (irrigation and precipitation), as these generally correspond to an abrupt increase in $K_{c\text{-}act}$ in response to increased evaporation (Torres and Calera, 2010). Specific concern is given thereafter to the beginning of the season since the soil is bare and consequently $K_{c\text{-}act}$ is dominated by K_e when an irrigation/precipitation event occurs. For this period, corresponds to a cover fraction < 0.2, the 4 days following the watering event are eliminated from the data base (Duchemin et al., 2006). Later in the season, K_e is assumed to be neglected compared to $K_{cb\text{-}act}$ as the vegetation is well developed and covers the soil (Allen et al., 1998; Duchemin et al., 2006). The effect of water stress can also affect the computation of the crop coefficient $K_{cb\text{-}act}$ during the period of full development (Pôças et al., 2020). The water stressed data are characterized by a drop of $K_{c\text{-}act}$ (Duchemin et al., 2006). In this study, the data lower than one standard deviation (of the mid-season period data average) is discarded. By this point, we assume that the remaining data correspond to $K_{c\text{-}act} = K_{cb\text{-}act}$.

ii) The relationships between $K_{cb\text{-}act}$ from one hand and ρ_{VV}, ρ_{VH}, PR and NDVI from the other hand are investigated for both fields and both seasons.

iii) Relationships are first established using data from 2017–2018 season (S1) over Field 1 and then used to derive $K_{cb\text{-}act}$ and consequently $ET_{c\text{-}act}$ over the other seasons/fields.

2.4. Satellite data

2.4.1. Sentinel-1 data

Sentinel-1 is a constellation composed of two satellites, Sentinel-1A launched in 2014 and Sentinel-1B launched in 2016. Each satellite is equipped with a C-band SAR sensor with a frequency of 5.33 GHz. The two satellites map the entire world in 175 orbits with a revisit time of six days (Torres et al., 2012). The operational mode IW (Interferometric Wide-swath mode) allows the acquisition of data in dual polarization (VV and VH) with an azimuth resolution of 20 m and a ground range resolution of 5 m (European space agency, 2012).

The Sentinel-1 Data Hub website (https://scihub.copernicus.eu) gives free access to two types of products: (i) SLC products (Single Look Complex) which are raw images that contain the radar measurement as a complex number and; (ii) GRDH products (Ground Range Detected High resolution) which are multi looked (to reduce the speckle) and projected to ground range to have square pixels that contains only a measurement of the intensity of the measured signal. The descending relative orbit number 52 maps the study area at 06:30 UTC with an incidence angle of about 35.2° over both fields. GRD and SLC products are used to compute the backscattering coefficient and the interferometric coherence, respectively, as described in the following sections. The data availability is illustrated in Fig. A1 in the Appendix. Please note that the relationships between radar and vegetation variables are not shown in this paper, as they have been already studied in detail in Ouaadi et al. (2021a). The reader is invited to consult this reference for more details on these relationships during the agricultural season.

2.4.1.1. Backscattering coefficient. The backscattering coefficient is computed from the GRDH products using the Orfeo toolbox (CNES,

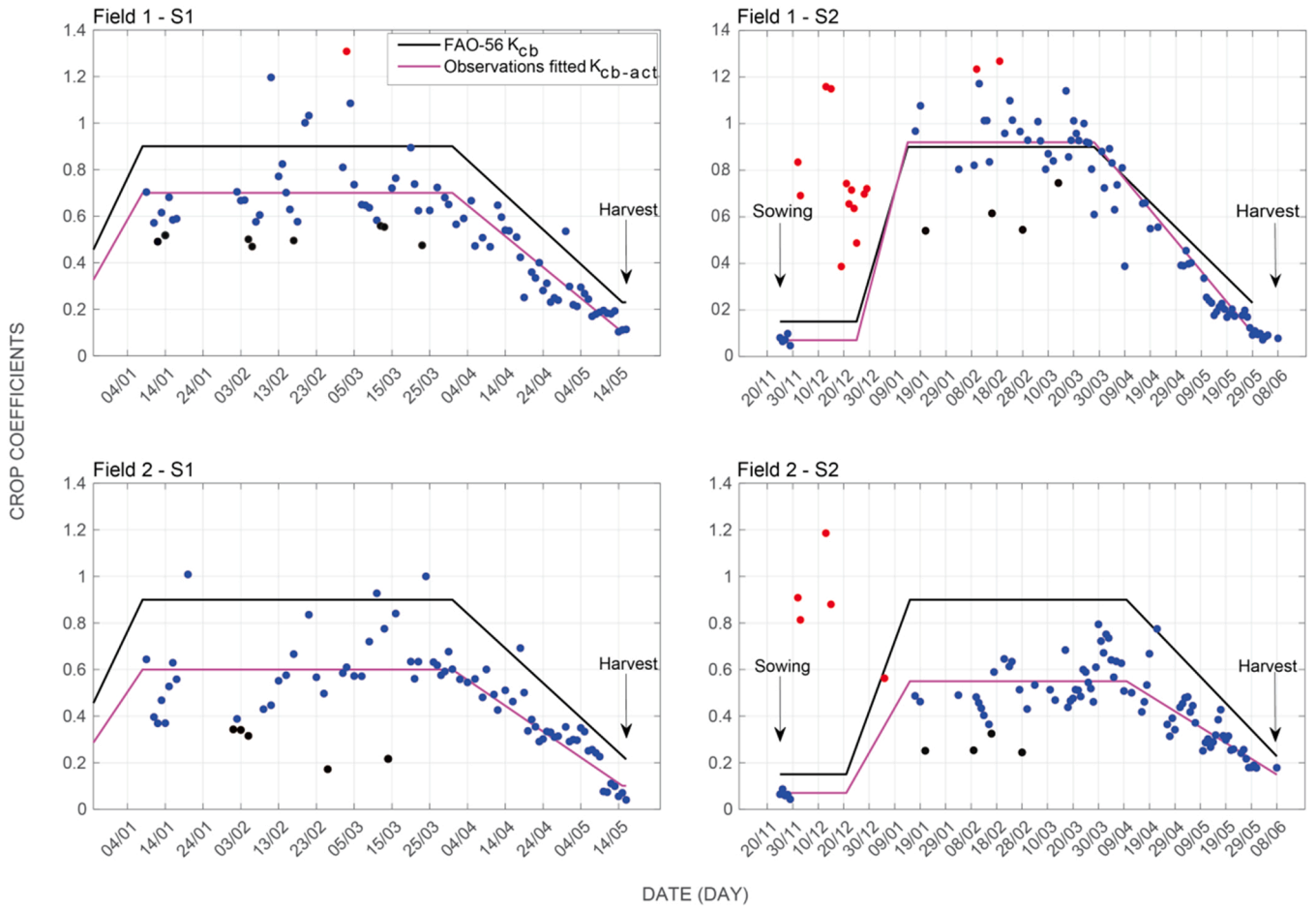

Fig. 3. Time series of crop coefficient $K_{c\text{-}act}$ over Field 1 and Field 2 for both seasons S1 and S2 (2016–2017 and 2017–2018, respectively). The red and black points correspond to points removed because of soil evaporation or vegetation water stress (see text for further details) and the remaining data correspond to $K_{c\text{-}act} = K_{cb\text{-}act}$. The $K_{cb\text{-}act}$ segmented curve obtained from the observations (blue points) is plotted in magenta. The K_{cb} curve using the FAO-56 tabulated values is also plotted in black for comparison purposes.

2018) with a processing chain that consists of three modules applied to each image for each polarization (Frison and Lardeux, 2018): *Thermal noise removal*, *Calibration* and *Terrain correction*. The last aims to project the images on the surface of the Earth using the digital terrain model SRTM (Shuttle Radar Topography Mission) at 30 m resolution. The obtained products are the backscattering coefficient at VV (σ^0_{VV}) and VH (σ^0_{VH}) with a spatial resolution of 10 m. Finally, the radar backscattering coefficient is obtained from averaging all the pixels values within a field. Details of the processing steps are provided in Ouaadi et al. (2021a).

The polarization ratio (PR) is calculated as the ratio between σ^0_{VH} and $\sigma^0_{VV}$and then converted to dB for a better visualization of the data dynamics.

2.4.1.2. Interferometric coherence. The interferometric coherence (ρ) is a complementary information to σ^0 and well correlated with vegetation development. Since it contains the phase information, the SLC products allows computing ρ by exploiting the repeated orbits of Sentinel-1: 6 days between two consecutive acquisitions using Sentinel-1 A and B of the same orbit. The combination of the two successive images allows measuring the change occurred to the scene between these two dates. The result is a scalar ranging between 0 when there is no correlation between the two images and 1 when the correlation is perfect. Over an agricultural area, the main cause of ρ decrease is the temporal decorelation caused by the change in orientation, size and position of the scatterers (canopy components). Indeed, it was found that the coherence is almost constant at high values (0.9 at VV) in summer when the soil is bare (Ouaadi et al., 2020) while the natural movement of vegetation components (leaves, stems.) under the effect of wind and rainfall in addition to the change caused by the growth of vegetation induce a gradual decrease in ρ to reach levels down to 0.2 during the agricultural season. It is worth mentioning that soil moisture change has also been shown to impact ρ in some cases (De Zan et al., 2014; Morrison et al., 2011; Scott et al., 2017) and does not highlight high impact on others (Ouaadi et al., 2020).

The Sentinel SNAP application platform is used to calculate the interferometric coherence at VV (ρ_{VV}) and VH (ρ_{VH}) based on a five steps processing chain: *Apply-Orbit-file*, *Back-geocoding*, *Coherence*, *TOPSAR-Deburst* and *Terrain-correction*. As for σ^0, ρ is obtained from averaging all the pixel values within a plot. For more details on the processing chain, the reader is referred to Ouaadi et al. (2021a).

2.4.2. Sentinel-2 NDVI

The Sentinel-2 is an optical constellation of two satellites Sentinel-2A launched on 2015 and Sentinel-2B launched on 2017, providing data on 13 spectral bands in the visible, near and medium infrared domains with a spatial resolution ranging from 10 to 60 m and a revisit time of 5 days. Over the study area, the data are atmospherically corrected using the MAJA chain developed at CESBIO (Hagolle et al., 2015). The products are freely distributed by the National Centre for Space Studies (CNES) via two platforms: PEPS (https://peps.cnes.fr) and Theia (https://theia.cnes.fr). Among the 45 available images over the two agricultural seasons, only 28 are free of clouds (less than 30 % of clouds) over the study

Table 2
Default FAO-56 and adjusted lengths of the crop growth stages over Field 1 and Field 2 and both seasons S1 (2016–2017) and S2 (2017–2018).

	FAO-56	Field 1		Field 2	
		S1	S2	S1	S2
L_{ini}	30	20	30	20	26
L_{dev}	140	23	21	23	26
L_{mid}	40	81	72	81	84
L_{late}	30	47	62	47	60
Total	240	171	185	171	196

area (see data availability in Fig. A1 in the Appendix). The 28 images are downloaded and processed to extract the NDVI (using the red and near infrared bands: bands 4 and 8) and finally an average per field is computed.

3. Results

The first section is devoted to crop coefficients analysis over the agricultural season. The second section is dedicated to the investigation of the relationships between $K_{cb\text{-}act}$ and remote sensing variables. Finally, the third section is dealing with the estimation of $K_{cb\text{-}act}$ and $ET_{c\text{-}act}$. The raw LE data are used but the results of $K_{cb\text{-}act}$ and $ET_{c\text{-}act}$ estimation with corrected LE are also reported.

3.1. Time series of the crop coefficients

Fig. 3 displays the time series of the crop coefficient obtained from the measured $ET_{c\text{-}act}$ over the two fields, during the two seasons S1 and S2. Sowing and harvest dates for each season are marked with arrows in the figure. For the season S1, data are available only from January 9.

The $K_{c\text{-}act}$ shape is a trapezoidal shape with low values at the start of the season when the soil is almost bare, increasing values during the development stage, a plateau of maximum values during the full development and then the $K_{c\text{-}act}$ decreases progressively at the end of the season with the senescence of the vegetation. The first values of $K_{c\text{-}act}$ around the sowing dates are very low probably because the soil is almost dry at this time. Thereafter, $K_{c\text{-}act}$ can reach high values in response to high evaporation (i.e. the red points in Fig. 3) because of rainfall and frequent irrigation (see Fig. 2 for rainfall and irrigation distribution) applied by the farmer to accelerate wheat emergence and development (Ouaadi et al., 2021b). Likewise, the $K_{c\text{-}act}$ values corresponding to water stress during the period of full development are presented in black. The red and black points are removed and it is assumed that the remaining data correspond to $K_s \sim 1$ and $K_e \sim 0$ and therefore $K_{c\text{-}act} = K_{cb\text{-}act}$. Considering the mean value for each stage (initial $K_{cb,init}$, mid-season $K_{cb,mid}$ and late season $K_{cb,end}$), the $K_{cb\text{-}act}$ segmented curve is constructed (magenta curve in Fig. 3) for each field and each season. For comparison purposes, the K_{cb} curve obtained using FAO-56 tabulated values, with crop stages duration adjusted based on the field observations and NDVI cycle is also displayed in black in Fig. 3. Table 2 reports the default FAO-56 and adjusted lengths of the crop growth stages (initial L_{init}, crop development L_{dev}, mid-season L_{mid} and late season L_{late}). Significant discrepancies are observed between the tabulated FAO-56 values and the adjusted values for the fields. This highlights the need for local calibration of FAO-56 as reported by many authors (Er-Raki et al., 2008; Pôças et al., 2020 among others, see Introduction).

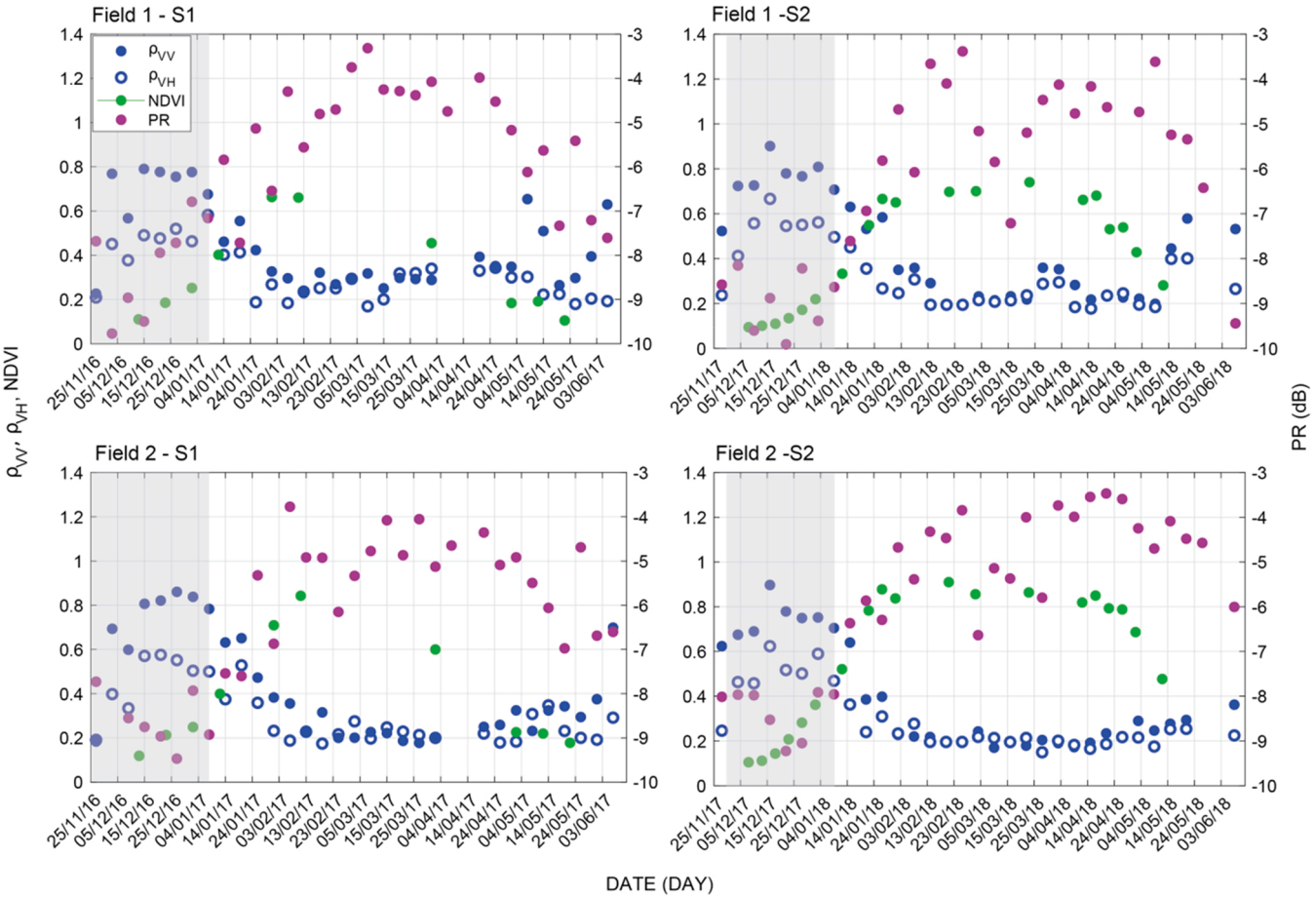

Fig. 4. Time series of the remote sensing variables including optical NDVI and radar PR, ρ_{VV} and ρ_{VH} over Field 1 and Field 2 and both seasons S1 (2016–2017) and S2 (2017–2018). The shaded area represents the period when $K_{c\text{-}act}$ points were removed due to soil evaporation (see red dots in Fig. 3).

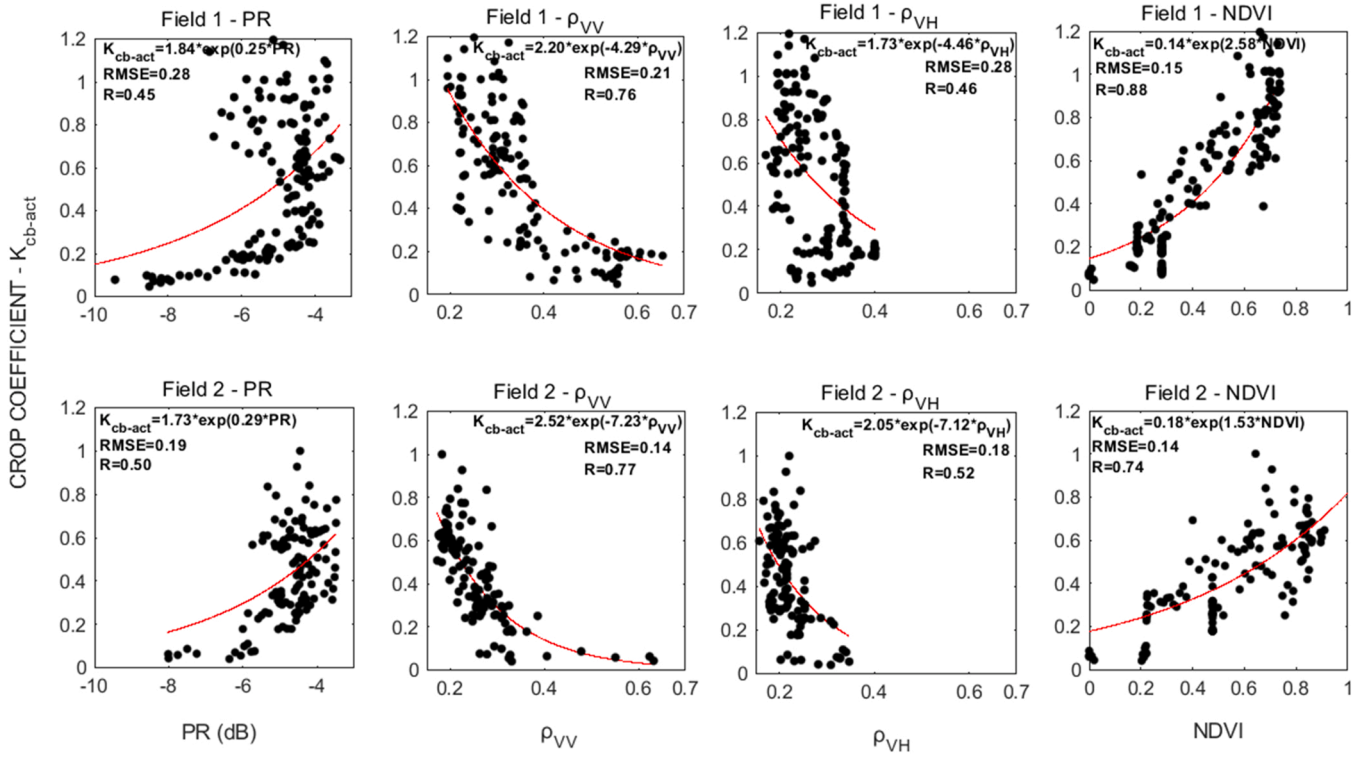

Fig. 5. Relationships between the satellite indices PR, ρ_{VV}, ρ_{VH} and NDVI with $K_{cb\text{-}act}$ for the two wheat fields Field 1 and Field 2. Each subplot contains data of the two agricultural seasons S1 (2016–2017) and S2 (2017–2018).

A value of $K_{cb,init} = 0.15$ is given in FAO-56 assuming that there is always some moisture in the soil, while in this study $K_{cb,init}$ is ~0.07 probably because the tilling is not deep and the soil surface is very dry (surface soil moisture average ~0.03 m^3/m^3 on 27/11/2017 over both fields). This is also the reason why the obtained K_{cb} at the end of the season (about 0.1–0.17) is lower than the FAO-56 value (0.23). For mid-season period, FAO-56 $K_{cb,mid}$ is equal to 0.9 which is close to the $K_{cb,mid}$ obtained over Field 1 during season S2, while the values obtained are lower for Field 2 and Field 1 S1. This is related to the combined effect of the meteorological conditions with cropping system and vegetation physiological properties (see the Introduction section). Indeed, the average of $K_{cb\text{-}act}$ reached at mid-season is different between the fields. During season S1, the average $K_{cb,mid}$ for both fields are close with 0.7 over Field 1 and 0.6 over Field 2. By contrast, noticeable differences between the two fields are observed during season S2, with significantly lower values of $K_{cb\text{-}mid}$ on Field 2. The higher $K_{cb\text{-}mid}$ over Field 1 during S2 compared to S1 could be attributed to the wetter conditions of the 2017–2018 growing season compared to the 2016–2017 season, resulting in much more vegetation as illustrated by the difference in the amount of biomass between the two seasons presented in Ouaadi et al. (2021a). On the other hand, the low values of $K_{cb\text{-}mid}$ on Field 2 are probably the result of the particular growing conditions of this field during S2 with a mixture of barley and wheat in addition to the high presence of adventices (see above). Indeed, $ET_{c\text{-}act}$ is highly affected by the specific canopy characteristics (geometric and physiological) such as the leaf arrangement, the height of the vegetation and stomata properties (Araya et al., 2011).

The time series of PR, ρ_{VV}, ρ_{VH} and NDVI over the four growing seasons are presented in Fig. 4. The evolution of these variables illustrates a seasonal evolution following the development of wheat. Early in the season, the values are low/high and start to increase/decrease with the development of the vegetation until a maximum/minimum value is reached in full development for NDVI/PR and interferometric coherences, respectively. With the onset of senescence, a progressive decreasing/increasing trend is observed until harvest. It can be pointed out that, for low values of ρ (≤ 0.4), corresponding to full development of vegetation, ρ_{VV} and ρ_{VH} are quite identical. However, for high values (≥ 0.4), corresponding to low vegetation, i.e. when vegetation is at early stage of development or during senescence, $\rho_{VV} \geq \rho_{VH}$, traducing the higher sensitivity of VH polarization to small amounts of vegetation. It should be kept in mind, however, that high values of the interferometric coherence (> 0.5) are more significant than the low values that are contaminated by noise.

3.2. *Relationships between $K_{cb\text{-}act}$ and satellite variables*

The relationships between $K_{cb\text{-}act}$ and the different radar data, including PR, ρ_{VV}, and ρ_{VH} (with the same x-axis scale 0.15–0.7 for ρ_{VV}, and ρ_{VH}) are presented in Fig. 5 for Field 1 and Field 2. The relationship between $K_{cb\text{-}act}$ and NDVI is also displayed to compare the performance of the radar variables with this commonly used optical index. Using the complete wheat cycle from sowing to harvest, the best fit is found to be exponential between $K_{cb\text{-}act}$ and all the satellite variables. The regression equation, R and RMSE calculated between the predicted variable using the fitted relationship (in red) and the observations are displayed in each subplot.

Results show that the best fitting is obtained between $K_{cb\text{-}act}$ and ρ_{VV} (hereafter named $K_{cb\text{-}act}$ - ρ_{VV}) and between $K_{cb\text{-}act}$ and NDVI ($K_{cb\text{-}act}$ - NDVI) regarding data from both fields. In contrast, the relationships are more scattered using ρ_{VH} ($K_{cb\text{-}act}$ - ρ_{VH}) and PR ($K_{cb\text{-}act}$ - PR). The problem is due to a significant dispersion of the data, in particular during the transition phase between the low/high plateaus values (see Fig. 4). PR was introduced to describe vegetation development while reducing the effect of soil variables on the backscattered signal, yet it seems to contain some of these effects. This may be related to a combined effect of wheat geometry and soil drying. After heading σ^0_{VH} is still high because of the volume contribution from the head layer while σ^0_{VV} is low and quite constant as the soil is dry. Consequently, the PR remained high late in the season.

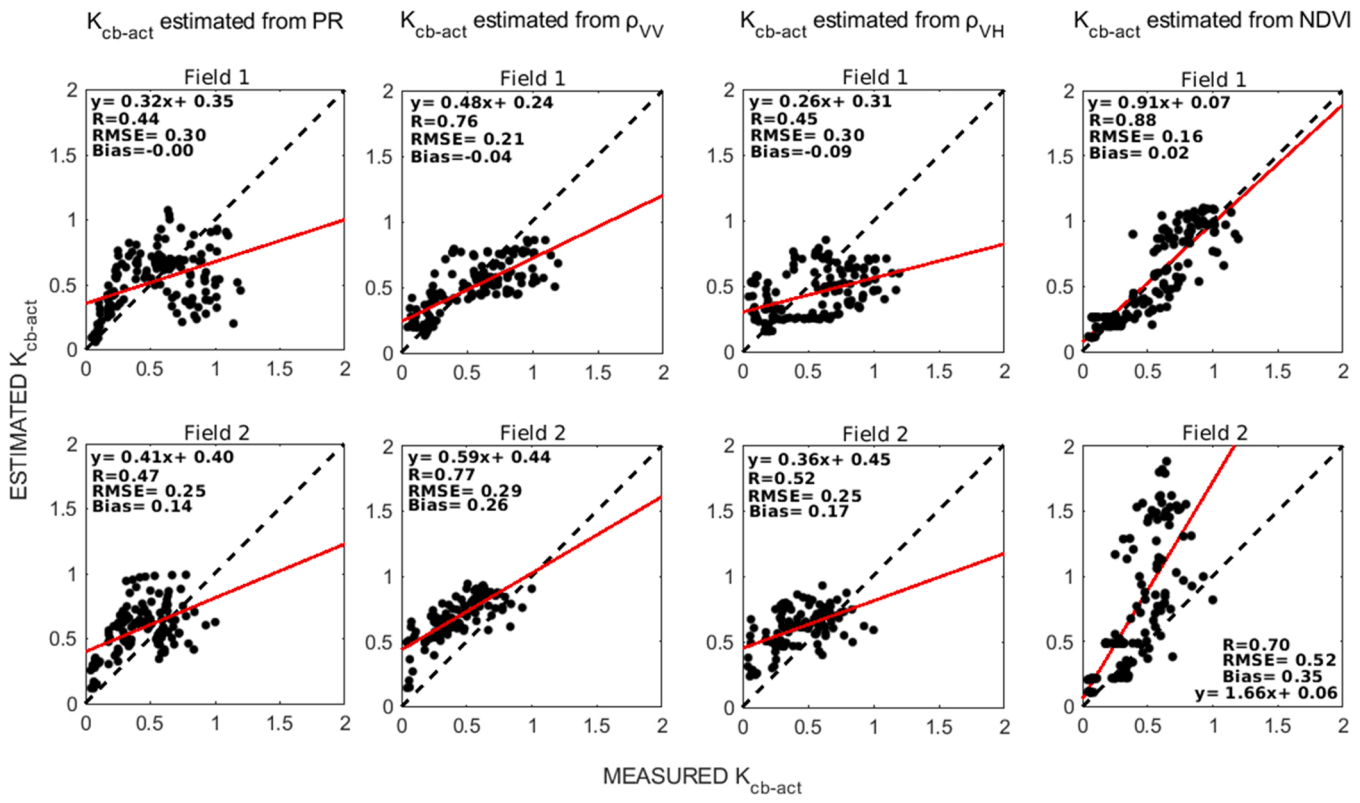

Fig. 6. Estimated versus measured $K_{cb\text{-}act}$ over Field 1 and Field 2 using the relationships $K_{cb\text{-}act}$ - PR, $K_{cb\text{-}act}$ - ρ_{VV}, $K_{cb\text{-}act}$ - ρ_{VH} and $K_{cb\text{-}act}$ - NDVI calibrated on Field 1 season 2017–2018 (S2).

The weak relationship with ρ_{VH} is not surprising due to the low overall values (≤ 0.4) which are less significant than ρ_{VV} (≤ 0.65). This is due to the highest sensitivity of VH polarization to low vegetation, leading to lowest coherence values at VH (Fig. 4). It is the reason why better relationship is observed for ρ_{VV} which show an amplitude of 0.45 ($0.2 \leq \rho_{VV} \leq 0.65$). It is interesting to note that ρ_{VH} and ρ_{VV} (when $\leq$ 0.35) are less scattered for Field 2 than for Field 1. Indeed, $K_{cb\text{-}act}$ is more scattered on Field 1, in particular, around mid-season when ρ_{VH} is at its lowest level ($\rho_{VH} < 0.33$). In general, the statistical metrics using the radar variables are better for Field 2 than for Field 1 because of the scattering of $K_{cb\text{-}act}$ around mid-season (Fig. 3). In contrast, the best metrics are obtained on Field 1 for $K_{cb\text{-}act}$ - NDVI, which are also the best metrics obtained for the 8 subplots investigated in this study with an RMSE limited to 0.15. This $K_{cb\text{-}act}$ - NDVI relationship is compared to similar relationships previously published: (1) Duchemin et al. (2006) have used a linear relationship: $K_{cb-act} = 1.64 * \mathrm{NDVI} - 0.14$; (2) Hunsaker et al. (2005) have fitted $K_{cb\text{-}act}$ to NDVI using a third-order regression model: $K_{cb-act} = 0.18 + 1.63\mathrm{NDVI}_n - 2.57\mathrm{NDVI}_n^2 + 1.93\mathrm{NDVI}_n^3$ with $NDVI_n = \frac{\mathrm{NDVI} - \mathrm{NDVI}_{min}}{\mathrm{NDVI}_{max} - \mathrm{NDVI}_{min}}$; (3) Er-Raki et al. (2007) derived $K_{cb\text{-}act}$ from NDVI using an exponential relationship: $K_{cb-act} = 1.07\left(1 - NDVI_m^{0.84/0.54}\right)$ with $NDVI_m = \frac{\mathrm{NDVI}_{max} - \mathrm{NDVI}}{\mathrm{NDVI}_{max} - \mathrm{NDVI}_{min}}$. Fig. A2 displays our observations and the different relationships including ours in red over Field 1. The different relationships provide with quite close results, the closest being provided by Duchemin et al. (2006) for wheat fields also grown in the Tensift catchment near Marrakech with similar climate conditions. Considering all the results of this study, $K_{cb\text{-}act}$ - NDVI provides good performance but the statistics of $K_{cb\text{-}act}$ - ρ_{VV}, comparable with those of $K_{cb\text{-}act}$ - NDVI, are also promising.

3.3. $K_{cb\text{-}act}$ and crop evapotranspiration estimation

In this section, $K_{cb\text{-}act}$ is estimated from different $K_{cb\text{-}act}$ - satellite variables relationships, and then the estimated $K_{cb\text{-}act}$ is used to calculate the $ET_{c\text{-}act}$. First, the data from one season (Field 1 season S2) was chosen to calibrate the 4 relationships (using the four variables PR, ρ_{VV}, ρ_{VH} and NDVI). This relationship is then used to estimate $K_{cb\text{-}act}$ over all fields/seasons. This season is chosen because the 2016–2017 season is not complete as previously mentioned. The results obtained are presented in Fig. 6 for both fields and both seasons.

As expected, the best results are obtained with $K_{cb\text{-}act}$ - NDVI and $K_{cb\text{-}act}$ -ρ_{VV}. Over Field 1, the retrieved $K_{cb\text{-}act}$ from radar data is limited to almost 1 because of the quick saturation of the C-band data while the $K_{cb\text{-}act}$ - NDVI can reach up to 1.2 and thus reproduce well the $K_{cb\text{-}act}$. This advantage is reflected on the good statics on this field with R = 0.88, slope = 0.91, RMSE = 0.16 and a bias limited to 0.02. However, this can also be a drawback from another point of view, obviously when the canopy is very dense and consists of a mixture of several vegetation types as is the case in Field 2. On this field, a significant overestimation (up to $K_{cb\text{-}act} = 2$) is observed with a reduction in statistical metrics to R = 0.70, slope = 1.66, RMSE = 0.52 and bias = 0.35. This can be explained by Fig. 4 and Fig. 3 where NDVI is higher in Field 2 than in Field 1 while $K_{cb\text{-}act}$ is lower in Field 2 than in Field 1. In fact, the low $K_{cb\text{-}act}$ values are obviously due to the lower $ET_{c\text{-}act}$ of season S1 of Field 2 compared to Field 1. This is due to the presence of adventices with two possible scenarios: (i) adventices do not transpire much which leads to a reduction in $ET_{c\text{-}act}$; (ii) adventices lead to a reduction in soil evaporation as they cover the entire soil. Indeed, the measured canopy cover (fc, not shown) shows high values since the beginning of the season where fc has reached 0.9 on 31/01/2018 on Field 2 versus 0.7 on Field 1 and had only reached 0.9 52 days later (13/03/2018). In contrast, the higher cover fraction of green vegetation (adventices and wheat) is obviously driven at a much higher NDVI than Field 1 and thus $K_{cb\text{-}act}$ is overestimated.

In contrast, similar statistical metrics are obtained between Field 1 and Field 2 using the radar variables. The statistical metrics of $K_{cb\text{-}act}$ -

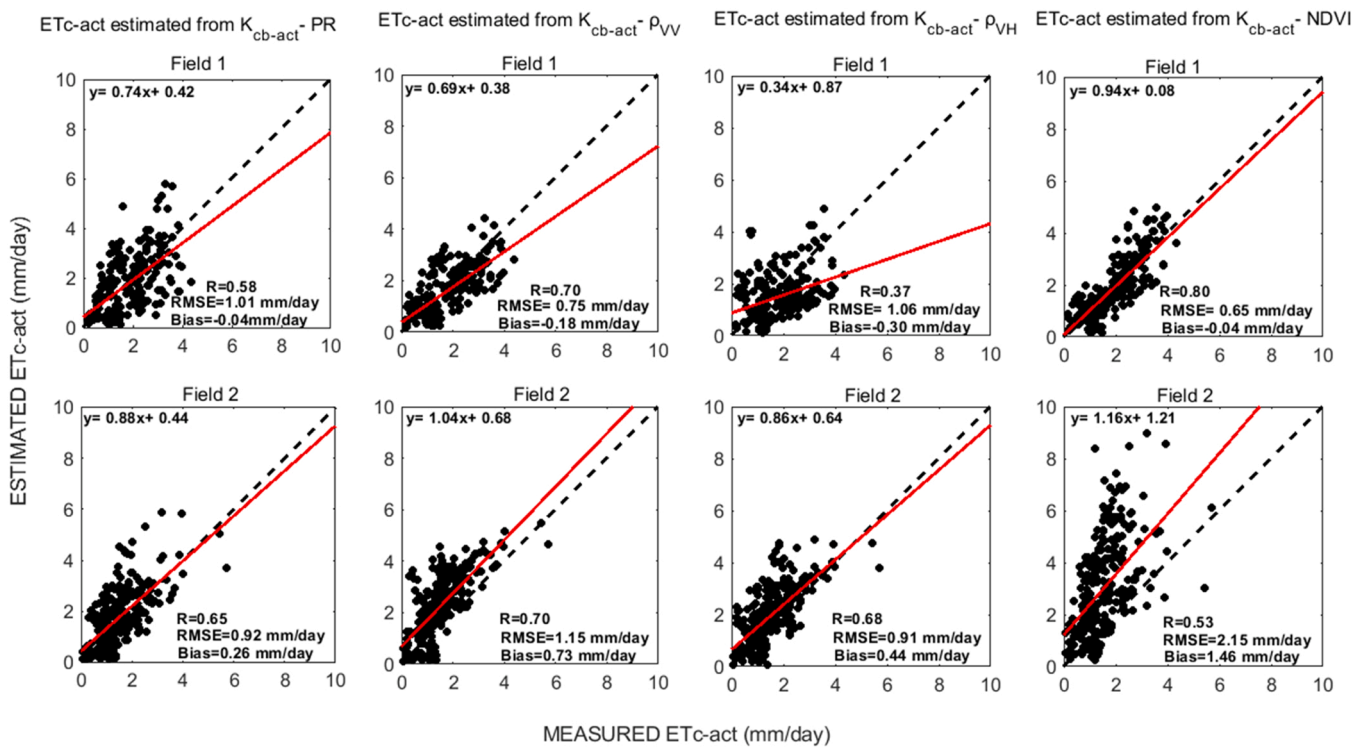

Fig. 7. Estimated versus measured $ET_{c\text{-}act}$ over Field 1 and Field 2 using the different relationships $K_{cb\text{-}act}$ - PR, $K_{cb\text{-}act}$ - ρ_{VV}, $K_{cb\text{-}act}$ - ρ_{VH} and $K_{cb\text{-}act}$ - NDVI.

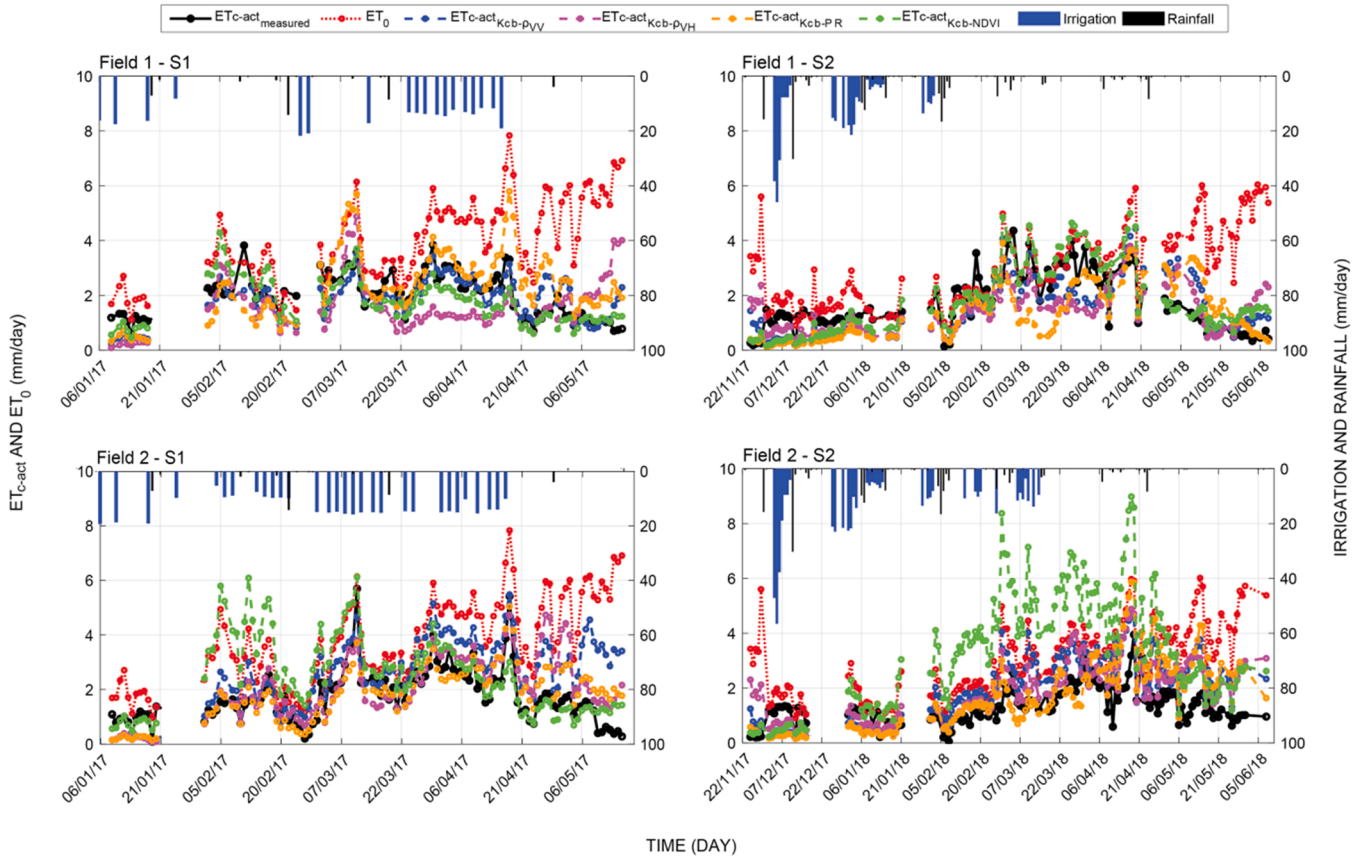

Fig. 8. Time series of estimated $ET_{c\text{-}act}$ using $K_{cb\text{-}act}$ derived from PR, ρ_{VV}, ρ_{VH} and NDVI superimposed to measured $ET_{c\text{-}act}$ and ET_0 ($K_{cb\text{-}act}$ is denoted by K_{cb} in the figure for simplification). Irrigation and precipitation amounts are also displayed.

ρ_{VV} are lower than $K_{cb\text{-}act}$ - NDVI for Field 1 but they are better for Field 2. In addition, $K_{cb\text{-}act}$ - ρ_{VV} demonstrates a more stable performance between the two fields where R = 0.76 and 0.77 for Field 1 and Field 2, respectively. Nevertheless, the bias is higher for Field 2, indicating a slight overestimation (y-intercept = 0.44). This was mainly attributed to the end of the season when the estimated $K_{cb\text{-}act}$ does not decrease enough to reach the lowest measured $K_{cb\text{-}act}$ values (not shown). The $K_{cb\text{-}act}$ - ρ_{VH} and $K_{cb\text{-}act}$ - PR provides with less accurate estimates with a better performance on Field 2 due to a lower scattering of $K_{cb\text{-}act}$ on this field as discussed in the previous section (Fig. 5).

Using the estimated $K_{cb\text{-}act}$, the $ET_{c\text{-}act}$ is then calculated and the results obtained for both fields are presented in Fig. 7. The outcomes with $K_{cb\text{-}act}$ - NDVI and $K_{cb\text{-}act}$ - ρ_{VV} are encouraging because of the good estimates of $K_{cb\text{-}act}$ (Fig. 6). Consequently, similar comments can be drawn. The $K_{cb\text{-}act}$ - NDVI has yielded very good estimate of $ET_{c\text{-}act}$ over Field 1 with R = 0.80 and RMSE = 0.65 mm/day for $ET_{c\text{-}act}$ values up to 4.5 mm/day.

As expected, the performance drops to R = 0.53 and bias = 1.46 mm/day over Field 2 and the RMSE increased from 0.65 to 2.15 mm/day due to the overestimation of $K_{cb\text{-}act}$, knowing that the maximum $ET_{c\text{-}act}$ is around 6 mm/day on Field 2. The stable estimate of $K_{cb\text{-}act}$ by the $K_{cb\text{-}act}$ - ρ_{VV} is reflected in the $ET_{c\text{-}act}$ estimation metrics where R is equal to 0.7 for both fields. However, the overestimation of $K_{cb\text{-}act}$ at the end of the season led to a higher RMSE on Field 2 (1.15 mm/day on Field 2 versus 0.75 mm/day on Field 1). Interestingly enough, $K_{cb\text{-}act}$ - PR and $K_{cb\text{-}act}$ - ρ_{VH} methods provided with similar metrics as $K_{cb\text{-}act}$ - NDVI and $K_{cb\text{-}act}$ - ρ_{VV} in estimating $ET_{c\text{-}act}$ even that the relationships used to estimate $K_{cb\text{-}act}$ are of poor quality (see Fig. 5 for $K_{cb\text{-}act}$ - PR and $K_{cb\text{-}act}$ - ρ_{VH} relationships). For instance, $K_{cb\text{-}act}$ - PR provided an estimate of $ET_{c\text{-}act}$ with R = 0.63, slope = 0.89, RMSE = 1.02 mm/day and bias = 0.38 mm/day over Field 2. This is probably related to the quasi-absence of water stressed period that could lead to strong discrepancies between $ET_{c\text{-}act}$ and ET_0 on these irrigated fields. Within these conditions, the inter-daily dynamics of $ET_{c\text{-}act}$ is mainly governed by ET_0 explaining the acceptable correlation coefficients for all the methods assessed in this study. To summarize, when passing from $K_{cb\text{-}act}$ - NDVI to $K_{cb\text{-}act}$ - radar variables, R was decreased by 12.5 % using ρ_{VV} and more than 27 % using PR and ρ_{VH} for Field 1. In contrast, R is improved on Field 2 using radar variables over NDVI with 24 % using ρ_{VV} and more than 18 % using PR and ρ_{VH}.

When corrected LE values are considered, the estimation of $K_{cb\text{-}act}$ and $ET_{c\text{-}act}$ over Field 1 and Field 2 yielded the statistical metrics summarized in Table A1 in the Appendix. The same approach as for raw LE values is adopted: (1) The relationships between $K_{cb\text{-}act}$ and different remote sensing variables are first computed using data of Field 1 S2; (2) $K_{cb\text{-}act}$ is estimated from these relationships and used to compute $ET_{c\text{-}act}$. The statistical metrics are close to those obtained with the raw data. The best relationships with $K_{cb\text{-}act}$ are obviously obtained with NDVI but using ρ_{VV} also provided with acceptable metrics. The main differences are related to higher biases leading to higher RMSE mainly on Field 1 while bias is lower on Field 2 when using NDVI.

For a temporal inter-comparison of the $ET_{c\text{-}act}$ estimated from different methods, Fig. 8 presents the time series of $ET_{c\text{-}act}$ estimated over Field 1 and Field 2 for the two agricultural seasons considering raw LE data. The ET_0, the measured $ET_{c\text{-}act}$, rainfall and irrigation are also displayed.

Results show good reproduction of the $ET_{c\text{-}act}$ time series especially using $K_{cb\text{-}act}$ - NDVI and $K_{cb\text{-}act}$ - ρ_{VV} for the Field 1 both seasons and Field 2 season S1. For Field 2 season S2, the presence of weed as well as the wind that laid down the high stems in April may be the reason for the low values obtained especially since the $ET_{c\text{-}act}$ estimated by the different methods is high. This highlights the effect of different growing conditions for the same crop planted in the same soil, in the same climate and with the same irrigation technique. Overall, the studies that have used NDVI (and other optical variables) so far have been conducted

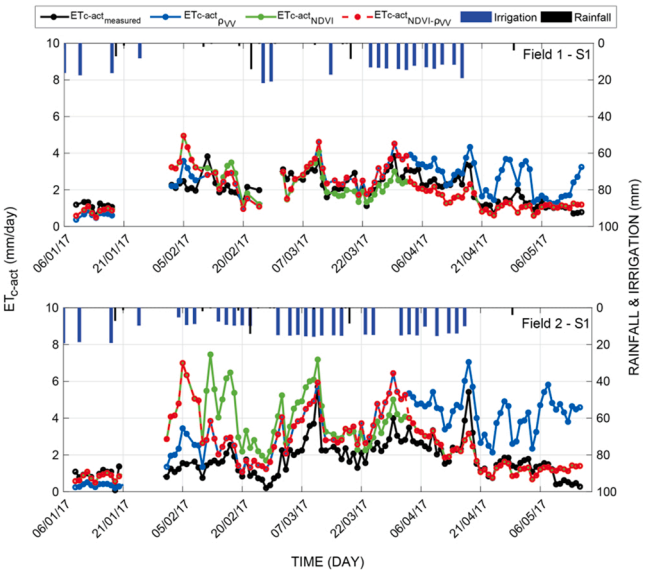

Fig. 9. Time series of $ET_{c\text{-}act}$ estimated from hybrid $K_{cb\text{-}act}$ over Field 1 and Field 2 season S1. The estimated $ET_{c\text{-}act}$ from $K_{cb\text{-}act}$ - NDVI and $K_{cb\text{-}act}$ - ρ_{VV} in addition to measured $ET_{c\text{-}act}$, rainfall and irrigation amounts are also displayed.

on fields with similar crop characteristics. The question of the generality of the relationships established to estimate $K_{cb\text{-}act}$ is still raised in previously published work. It has been reported that the effect of geometric properties, plant structure and development on $ET_{c\text{-}act}$ varies not only between crops but also between varieties of the same crop (Araya et al., 2011; Campos et al., 2017; Pôças et al., 2020) and thus may change if the crop is mixed with another type of vegetation such as adventices in our case.

By comparing the estimated $ET_{c\text{-}act}$ from the $K_{cb\text{-}act}$ retrieved from different satellite data, a slight underestimation is observed at the beginning of the season for the radar variables, which is due to the low estimated $K_{cb\text{-}act}$ compared to the NDVI that seems to estimate correctly the start of the season but then switches to a slight overestimation (clearly visible in Field 2 S1). This is in agreement with the results of French et al. (2020) using $K_{cb\text{-}act}$ estimated from Sentinel 2 and Venus (Dick et al., 2022) NDVI where they found that the performance is less accurate during the first 60 days after sowing. The authors who conducted their study at 7 different wheat fields in USA have reported accurate ET estimates from mid-season onwards. The significant overestimation observed on Field 2 (Fig. 6) is illustrated in Fig. 3. Even though Field 2 during season S2 presents some specific growing conditions as already mentioned, the estimated $ET_{c\text{-}act}$ is much higher than the ET_0 and this is due to the high $K_{cb\text{-}act}$ values caused by high NDVI values as discussed earlier. However, many shortcomings are highlighted in the literature concerning NDVI even though it is widely used (Huete, 1988; Huete et al., 2002; Huete and Liu, 1994; Pôças et al., 2020).

Among ρ_{VV}, ρ_{VH}, and PR, it appears that $K_{cb\text{-}act}$ - ρ_{VV} provides better results for $ET_{c\text{-}act}$ estimation until senescence. At this time of the season, even though the change in cover structure has stopped and the water content of the vegetation is low (water content is about 27 % of total biomass in Field 1 season 1), the coherence is generally still low due to the movement of scatters (wheat components), which leads to high $K_{cb\text{-}act}$ values and, consequently, high $ET_{c\text{-}act}$ values. This sensitivity of coherence to scatterers motion explains also the underestimation of $ET_{c\text{-}act}$ by ρ_{VV} and ρ_{VH} between 22/03/2018 and 06/04/2018 where an increase in ρ_{VV} and ρ_{VH} is observed (Fig. 4). Such anomalies could be avoided in future works by a simple smoothing.

Table 3
Statistical metrics of the estimated $ET_{c\text{-}act}$ using the $K_{cb\text{-}act}$ - NDVI relationship and using the hybrid $K_{cb\text{-}act}$ over Field 1 and Field 2 season S1.

	$K_{cb\text{-}act}$ - NDVI		Hybrid $K_{cb\text{-}act}$	
	Field 1 – S1	Field 2 – S1	Field 1 – S1	Field 2 –S1
R	0.69	0.53	0.74	0.63
RMSE (mm/day)	0.71	1.83	0.71	1.43
Bias (mm/day)	0.11	1.11	-0.04	-0.81

4. Discussion

So far, the research and efforts in estimating $K_{cb\text{-}act}$ have been focused only on using optical data. This is mainly due to the intrinsic simplicity and ease of interpretation and understanding of these indices (Pôças et al., 2020) that have made their use widespread for irrigation assessment; in particular, they can be used by technicians and farmers (Allen et al., 2011). In addition, they demonstrated good results in the estimation of $ET_{c\text{-}act}$. However, the continuous availability of optical time series throughout the agricultural season is prevented by cloudy conditions. This has led some researchers to seek alternative solutions for estimating vegetation indices when significant data gaps are presented. One of the most prominent approaches has been the consideration of radar data to fill these gaps (Filgueiras et al., 2019). Our results in this study show encouraging prospects for using radar data instead of optical indices for $ET_{c\text{-}act}$ estimation. Yet, it is also feasible to use the radar as a complement to the optics. For instance, Sentinel-2 images for the period from 11/02/2017–02/04/2017 are not useful due to cloud cover. Therefore, $K_{cb\text{-}act}$ is estimated from ρ_{VV} for this period and the rest is estimated from NDVI (hereafter called hybrid $K_{cb\text{-}act}$). Fig. 9 shows the estimated $ET_{c\ -act}$ from the hybrid $K_{cb\text{-}act}$ for Field 1 and Field 2. For comparison, the estimated $ET_{c\text{-}act}$ from $K_{cb\text{-}act}$ - NDVI, $K_{cb\text{-}act}$ - ρ_{VV} and the measured $ET_{c\text{-}act}$ are also shown in the figure. The corresponding statistical metrics are presented in Table 3. The results show an obvious improvement in the estimation of $ET_{c\text{-}act}$ using the hybrid $K_{cb\text{-}act}$ where an improvement of 6.7 % and 15.9 % on Field 1 and Field 2, respectively in the correlation is obtained. Interestingly, the bias is reduced by 63.6 % on Field 1 and the RMSE and bias are reduced by 21.8 % and 27 %, respectively, on Field 2 when using the hybrid $K_{cb\text{-}act}$. The use of $K_{cb\text{-}act}$ estimated from ρ_{VV} for the cloudy period reduced the overestimation by the $K_{cb\text{-}act}$ - NDVI over Field 2, clearly observed in the $ET_{c\text{-}act}$ time series between 05/02 and 15/03 in Fig. 9.

In addition to a hybrid approach that uses the radar and optical variables separately, it can be expected that combining both through multiple linear regression or machine learning algorithms would be a promising way to improve the estimation of $K_{cb\text{-}act}$.

However, it is worth mentioning that radar data are relatively more complicated to process and interpret than optical data, which can be a problem for direct applications by managers, although these difficulties are decreasing thanks to the rapid evolution of electronic equipment and platforms that can process radar data on a large scale and make them available to users. For example, the CNES platform (https://peps.cnes.fr) can now offer σ^0 maps on demand. Google earth Engine also provides large-scale products using free scripts found on the internet. It is hoped that these efforts will increase and make the processed data easily available to users who are not primarily radar data specialists.

This work is the first step in its concept and further research is obviously required. Here, the simple $K_{cb\text{-}act}$ approach is used as a first step to check the accuracies and potential use of different radar variables. The simple $K_{cb\text{-}act}$ approach is generally preferred because it allows for rapid analysis and rough quantification of $ET_{c\text{-}act}$ with relatively moderate accuracy of vegetation water stress and soil evaporation. On one hand, it is an approach well suited for large-scale agricultural water management. For instance, it can be used for irrigation scheduling by estimating K_{cb} from the proposed approach and the water stress coefficient K_s estimated, typically, from a water balance model such as the two-layer soil budget of the FAO-56 double coefficient approach. However, for operational irrigation management at large scale, the estimation of K_s from the water balance model is limited by the unavailability of irrigation data at the field scale over most irrigated areas as well as the difficulty in modeling the root zone soil moisture because of uncertain root depth and soil texture (Olivera-Guerra et al., 2018). Consequently, several studies have assessed the potentialities of thermal infrared data to estimate K_s (e.g. Ihuoma and Madramootoo, 2017; Kullberg et al., 2016; Olivera-Guerra et al., 2018). On the other hand, a better description of physical processes is beneficial. Our current work focuses on the partition of evaporation from the soil and the transpiration component. This approach, which is based on the resolution of the soil water balance, should also be corrected using K_s. This application would be very interesting and compatible with the resolution of Sentinels 1 and 2 with the upcoming availability of high spatio-temporal resolution of thermal data with the launch of future missions such as HyspIRI (2022), Sentinel-8 (2024), TRISHNA (2025) and LSTM (2028).

The transferability of the obtained relationships between $K_{cb\text{-}act}$ and remote sensing variables is a key issue. The FAO-56 been a very conceptual model, the relationships between $K_{cb\text{-}act}$ and NDVI (as NDVI is the most commonly used variable to estimate $K_{cb\text{-}act}$ in the literature), are well known to be specific to the site/region where they have been established. This is because $K_{cb\text{-}act}$ take into account all factors that make a specific crop different from the reference grass including development stage, density, geometry and health. It also depends on climate and on agricultural practices, as discussed in the introduction. As such, the domain of application of the $K_{cb\text{-}act}$ relationships with radar variables presented in this study should be limited to wheat under similar semi-arid climate and agricultural practices. To extend the genericity of the method by developing relationships for other conditions, a larger data base should be used.

From another perspective, the study should be extended to include other annual crops such as tree crops where the seasonal evolution of ρ and σ^0 (hence PR) is limited (Frison et al., 2018). Also, the investigation should be extended to other sites with different irrigation techniques such as flooding and sprinkling. Some studies have shown sensitivity of ρ to soil moisture such as Morrison et al. (2011) who demonstrated a relationship between ρ and soil moisture on bare soil in C-band. Similarly, De Zan et al. (2014) found a loss of ρ in response to increasing and decreasing soil moisture levels using L-band data on bare fields. For our database, no significant sensitivity to soil moisture is observed (details on Ouaadi et al., 2020). On one hand, this could be related to the low fraction of wetted soil surface (fw) as the fields are drip irrigated (fw = 0.3 (Allen et al., 1998)) compared to other techniques such as flooding where fw is equal to 1. On the other hand, it is most likely that in the presence of vegetation, the effect of soil moisture is negligible compared to the decorelation (or loss of ρ) caused by the vegetation. Indeed, Moeremans and Dautrebande (2000) reported that some ρ changes can be related to soil moisture variations on bare soils but these changes become negligible when the soil is vegetated. Similarly, Barrett et al. (2012) found that the effect of soil moisture variation is suppressed by the predominant effect of vegetation, particularly for C-band which is sensitive to both soil and vegetation characteristics (Ulaby et al., 1986). Using C- and L-band data, Molan and Lu (2020) also revealed that ρ is not related to changes in soil moisture over agricultural fields. However, it should be kept in mind that ρ is calculated in these studies, as in ours, with a minimum of 6 days between the two images (baseline), which is largely sufficient for agricultural cover to grow and, in most cases, weather conditions change, which will be the main sources of ρ loss. Stated differently, soil moisture could have an observable impact if ρ is calculated with a short baseline where the temporal development of vegetation is limited. Indeed, the experiment conducted by Albinet et al. (2016) on a tree demonstrated that watering the tree leads to an abrupt decrease in ρ that requires between 30 min and 6 h (depending on polarization) to recover the previous level before watering. From another

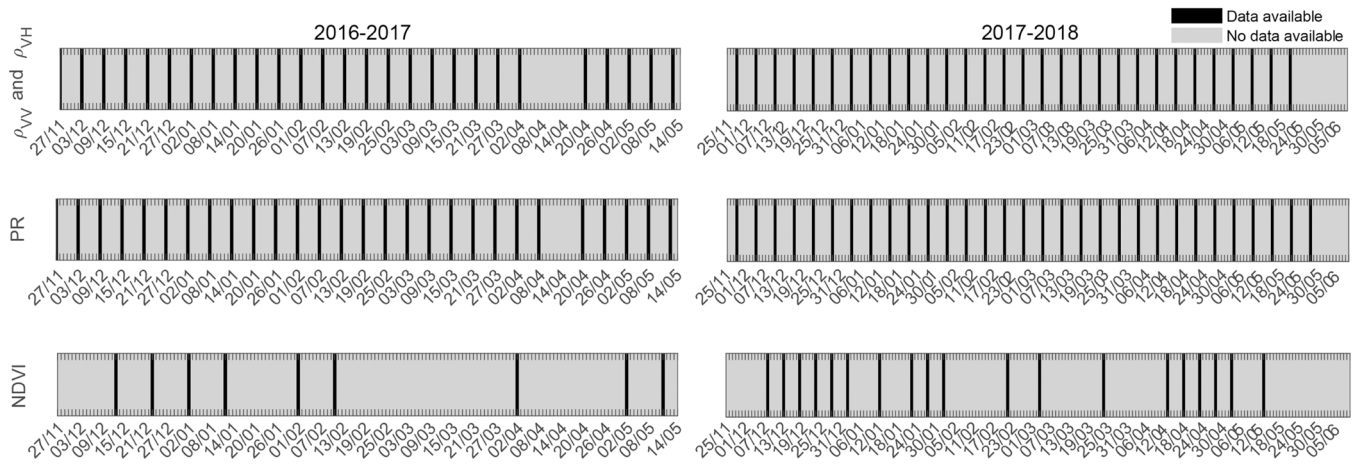

Fig. A1. Schedule of the remote sensing data availability (ρ_{VV}, ρ_{VH}, PR and NDVI) during the two agricultural seasons 2016–2017 and 2017–2018.

perspective, the results of Albinet et al. (2016) shows that the presence of water on the surface of vegetation components, due to watering events such as artificial or natural rainfall or due to dew, disrupts ρ. This was highlighted in the tropical forest by Hamadi et al., (2014). The further investigation of these different circumstances is necessary for a better evaluation of the $K_{cb\text{-}act}$ - ρ relationships since the degradation of ρ will automatically induce a degradation of the $K_{cb\text{-}act}$ - ρ relationships. In this context, sub-daily measurements of radar data over annual crops are needed to understand the impact of soil moisture on ρ. An experiment is currently installed in Morocco to measure ρ and σ^0 over a wheat field with a step of 15 min. The data are being processed and will be used in our future work.

5. Conclusions

This work seeks to evaluate the potential use of SAR data to estimate the crop coefficient $K_{cb\text{-}act}$ and crop evapotranspiration $ET_{c\text{-}act}$. The commonly used NDVI is also considered for comparison purposes. The study was conducted over four agricultural seasons of irrigated winter wheat in Morocco. Radar variables are estimated from the C-band Sentinel-1 sensor with a revisit time of 6 days and a resolution of 10 m. The NDVI is derived from Sentinel-2 with similar resolutions. First, the relationship between $K_{cb\text{-}act}$ on one hand and PR, ρ_{VV} and ρ_{VH} on the other hand is studied for the whole agricultural season. Second, the relationships $K_{cb\text{-}act}$ - PR, $K_{cb\text{-}act}$ - ρ_{VV} $K_{cb\text{-}act}$ - ρ_{VH} and $K_{cb\text{-}act}$ - NDVI are calibrated using an agricultural season and the derived relationships are used to estimate $K_{cb\text{-}act}$ and $ET_{c\text{-}act}$ over the four seasons.

The outcomes of this study showed that the variables derived from the SAR data can also be successfully used to estimate $K_{cb\text{-}act}$ and $ET_{c\text{-}act}$, in particular, $ET_{c\text{-}act}$ is estimated using $K_{cb\text{-}act}$ - ρ_{VV} with an RMSE = 0.75 mm/day which is close to the RMSE obtained using $K_{cb\text{-}act}$ - NDVI (RMSE = 0.65 mm/day) over Field 1. In contrast, RMSE values have increased to 1.15 mm/day versus 2.15 mm/day using $K_{cb\text{-}act}$ - $\rho_{VV}$and $K_{cb\text{-}act}$ - NDVI, respectively on Field 2 due to the specific growing conditions of this field with a high presence of adventices. However, based on our results, the radar variables and in particular ρ_{VV} demonstrates good performance and, in particular, a stability of the statistical metrics from one field and one season to another in the estimation of $ET_{c\text{-}act}$ over the two fields. This opens new perspectives for robust and operational applications at large spatial scales, especially in regions where optical data are inoperable or for crops grown in winter usually characterized by frequent cloudy conditions. Most importantly, the shortcomings obtained for $ET_{c\text{-}act}$ estimation using radar data are at the end of the season, a period that is not important for $ET_{c\text{-}act}$ applications and crop water requirement management since vegetation dries out at this time and irrigation is already stopped. The results also show that radar can be used as a complement to optics; in particular, the use of $K_{cb\text{-}act}$-derived from ρ_{VV} during the period of unavailability of optical images improved the correlation coefficient of $ET_{c\text{-}act}$ estimate by 7–16 % and reduced the bias by over 27 %. Our study presents the first attempt at estimating $K_{cb\text{-}act}$ and $ET_{c\text{-}act}$ from SAR data but further work is required for additional validation of the results as well as for a better and deeper investigation of the behavior of the $K_{cb\text{-}act}$-radar and $K_{cb\text{-}act}$-optical variables relationships and their robustness in estimating $ET_{c\text{-}act}$ when the geometrical and physiological properties of the canopy change as for example the case presented by season S2 of Field 2.

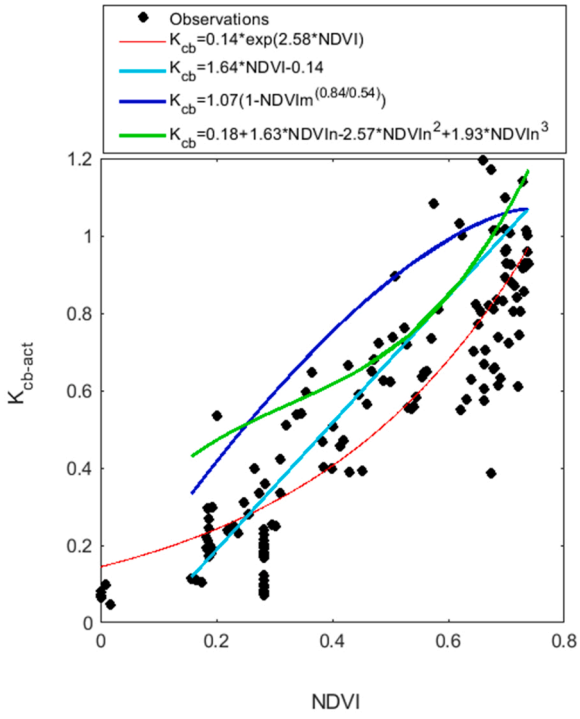

Fig. A2. Examples of $K_{cb\text{-}act}$ – NDVI relationships available in the literature for wheat crops over Field 1. The one established in this work is also superimposed in red ($NDVI_m = \frac{NDVI_{max} - NDVI}{NDVI_{max} - NDVI_{min}}$, $NDVI_n = \frac{NDVI - NDVI_{min}}{NDVI_{max} - NDVI_{min}}$).

Declaration of Competing Interest

The authors declare that they have no known competing financial interests or personal relationships that could have appeared to influence

Table A1
Statistical metrics obtained for the estimation of $K_{cb\text{-}act}$ and $ET_{c\text{-}act}$ after applying Bowen correction to the LE measurements ($K_{cb\text{-}act}$ is denoted by K_{cb} for simplification).

		Field 1				Field 2			
		K_{cb}-PR	K_{cb}-ρ_{VV}	K_{cb}-ρ_{VH}	K_{cb}-NDVI	K_{cb}-PR	K_{cb}-ρ_{VV}	K_{cb}-ρ_{VH}	K_{cb}-NDVI
$K_{cb\text{-}act}$ estimation	R	0.53	0.76	0.38	0.85	0.42	0.80	0.57	0.80
	RMSE (mm/day)	0.44	0.41	0.49	0.44	0.47	0.33	0.40	0.32
	Bias (mm/day)	-0.17	-0.24	-0.24	-0.34	-0.25	-0.11	-0.17	-0.10
$ET_{c\text{-}act}$ estimation	R	0.43	0.62	0.25	0.74	0.53	0.66	0.61	0.65
	RMSE (mm/day)	1.71	1.65	1.92	1.83	1.68	1.30	1.44	1.41
	Bias (mm/day)	-0.91	-1.14	-1.09	-1.50	-0.96	-0.51	-0.68	-0.40

the work reported in this paper.

Data Availability

Data will be made available on request.

Acknowledgements

The datasets used in this work were carried out within the frame of the International Joint Laboratory TREMA (https://www.lmi-trema.ma/). N.O. was funded by the ANR-19-CE01-0017 HILIAISE projects. The authors thank the financial support of the projects ERANET-MED CHAAMS, TOSCA/CNES MOCTAR and Rise-H2020-ACCWA. The authors are grateful to Theia for producing and distributing Sentinel-2 images corrected from atmospheric effects and to ESA for providing Sentinel-1 products free of charge. Finally, we would like to acknowledge Dr. Omar Rafi, the owner of the private farm for his long-time support for our research activities.

Appendix

See. Figs. A1-A2.
See. Table A1.

References

Abourida, A., Simonneaux, V., Errouane, S., Sighir, F., Berjami, B., Sgir, F., 2008. Estimation des volumes d'eau pompés dans la nappe pour l'irrigation (Plaine du Haouz, Marrakech, Maroc). Comparaison d'une méthode statistique et d'une méthode basée sur l'utilisation de données de télédétection. J. Water Sci. 21, 489–501.

Ait Hssaine, B., Merlin, O., Ezzahar, J., Ojha, N., Er-raki, S., Khabba, S., 2020. An evapotranspiration model self-calibrated from remotely sensed surface soil moisture , land surface temperature and vegetation cover fraction : application to disaggregated SMOS and MODIS data. Hydrol. Earth Syst. Sci. 24, 1781–1803. https://doi.org/10.5194/hess-24-1781-2020.

Ait Hssaine, B., Merlin, O., Rafi, Z., Ezzahar, J., Jarlan, L., Khabba, S., Er-raki, S., 2018. Calibrating an evapotranspiration model using radiometric surface temperature, vegetation cover fraction and near-surface soil moisture data. Agric. . Meteorol. 257, 104–115. https://doi.org/10.1016/j.agrformet.2018.02.033.

Ait Hssaine, B., Chehbouni, A., Er-raki, S., Khabba, S., Ezzahar, J., Ouaadi, N., Ojha, N., Rivalland, V., Merlin, O., 2021. On the utility of high-resolution soil moisture data for better constraining thermal-based energy balance over three semi-arid agricultural areas. Remote Sens 13, 727. https://doi.org/10.3390/rs13040727.

Alam, M.S., Lamb, D.W., Rahman, M.M., 2018. A refined method for rapidly determining the relationship between canopy NDVI and the pasture evapotranspiration coefficient. Comput. Electron. Agric. 147, 12–17. https://doi.org/10.1016/j.compag.2018.02.008.

Albinet, C., Borderies, P., Floury, N., Pottier, E., 2016. Measure of temporal variation of P-band radar cross section and temporal coherence of a temperate tree. IEEE Trans. Geosci. Remote Sens. 54, 6255–6264. https://doi.org/10.1109/TGRS.2016.2565384.

Allen, R.G., Pereira, L.S., Raes, D., Smith, M., 1998. Crop Evapotranspiration—Guidelines for Computing Crop Water Requirements, FAO Irrigation and Drainage Paper No. 56. FAO, ROME, Italy.

Allen, R.G., Tasumi, M., Trezza, R., 2007. Satellite-based energy balance for mapping evapotranspiration with internalized calibration (METRIC)—model. J. Irrig. Drain. Eng. 133, 380–394. https://doi.org/10.1061/(asce)0733-9437(2007)133:4(380).

Allen, R.G., Pereira, L.S., Howell, T.A., Jensen, M.E., 2011. Evapotranspiration information reporting: I. Factors governing measurement accuracy. Agric. Water Manag. https://doi.org/10.1016/j.agwat.2010.12.015.

Anapalli, S.S., Fisher, D.K., Pinnamaneni, S.R., Reddy, K.N., 2020. Quantifying evapotranspiration and crop coefficients for cotton (Gossypium hirsutum L.) using an eddy covariance approach. Agric. Water Manag. 233, 106091 https://doi.org/10.1016/j.agwat.2020.106091.

Annandale, J., Benade, N., Jovanovic, N., Steyn, J., 1999. Facilitating irrigation scheduling by means of the soil water balance model.

Araya, A., Habtu, S., Haile, M., Sisay, F., Dejene, T., 2011. Determination of local barley (hordeum vulgare) crop coefficient and comparative assessment of water productivity for crops grown under the present pond water in Tigray, Northern Ethiopia. Momona Ethiop. J. Sci. 3, 65–79. https://doi.org/10.4314/mejs.v3i1.63686.

Barrett, B., Whelan, P., Dwyer, N., 2012. The Use of C- and L-band repeat-pass interferometric SAR coherence for soil moisture change detection in vegetated areas. Open Remote Sens. J. 5, 37–53. https://doi.org/10.2174/1875413901205010037.

Bausch, W.C., 1993. Soil background effects on reflectance-based crop coefficients for corn. Remote Sens. Environ. 46, 213–222. https://doi.org/10.1016/0034-4257(93)90096-G.

Bausch, W.C., Neale, C.M.U., 1987. Crop coefficients derived from reflected canopy radiation: a concept. Trans. Am. Soc. Agric. Eng. 30, 703–709. https://doi.org/10.13031/2013.30463.

Bigeard, G., Coudert, B., Chirouze, J., Er-Raki, S., Boulet, G., Ceschia, E., Jarlan, L., 2019. Ability of a soil-vegetation-atmosphere transfer model and a two-source energy balance model to predict evapotranspiration for several crops and climate conditions. Hydrol. Earth Syst. Sci. 23, 5033–5058. https://doi.org/10.5194/hess-23–5033-2019.

Blaes, X., Defourny, P., 2003. Retrieving crop parameters based on tandem ERS 1/2 interferometric coherence images. Remote Sens. Environ. 88, 374–385. https://doi.org/10.1016/j.rse.2003.08.008.

Boudhar, A., 2009. Télédétection du manteau neigeux et modélisation de la contribution des eaux de fonte des neiges aux débits des Oueds du Haut Atlas de Marrakech. Cadi Ayyad University of Marrakech.

Busquier, M., Lopez-Sanchez, J.M., Mestre-Quereda, A., Navarro, E., González-Dugo, M. P., Mateos, L., 2020. Exploring TanDEM-X interferometric products for crop-type mapping. Remote Sens. 12, 1774. https://doi.org/10.3390/rs12111774.

Campos, I., Neale, C.M.U., Suyker, A.E., Arkebauer, T.J., Gonçalves, I.Z., 2017. Reflectance-based crop coefficients REDUX: for operational evapotranspiration estimates in the age of high producing hybrid varieties. Agric. Water Manag. 187, 140–153. https://doi.org/10.1016/j.agwat.2017.03.022.

Chaponnière, A., Boulet, G., Chehbouni, A., Aresmouk, M., 2008. Understanding hydrological processes with scarse data in a mountain environment. Hydrol. Process. 22, 1908–1921.

Chintala, S., Harmya, T.S., Kambhammettu, B.V.N.P., Moharana, S., Duvvuri, S., 2022. Modelling high-resolution Evapotranspiration in fragmented croplands from the constellation of Sentinels. Remote Sens. Appl. Soc. Environ. 26, 100704. https://doi.org/10.1016/j.rsase.2022.100704.

CNES, 2018. The ORFEO Tool Box Software Guide.

Coltelli, M., Fornaro, G., Franceschetti, G., Lanari, R., Migliaccio, M., Moreira, J.R., Papathanassiou, K.P., Puglisi, G., Riccio, D., Schwäbisch, M., 1996. SIR-C/X-SAR multifrequency multipass interferometry: a new tool for geological interpretation. J. Geophys. Res. E Planets 101, 23127–23148. https://doi.org/10.1029/96JE01301.

Courault, D., Seguin, B., Olioso, A., 2005. Review on estimation of evapotranspiration from remote sensing data: from empirical to numerical modeling approaches. Irrig. Drain. Syst. 19, 223–249.

De Zan, F., Parizzi, A., Prats-Iraola, P., López-dekker, P., 2014. A SAR interferometric model for soil moisture. IEEE Trans. Geosci. Remote Sens. 52, 418–425. https://doi.org/10.1109/TGRS.2013.2241069.

Diarra, A., Jarlan, L., Er-Raki, S., Le Page, M., Aouade, G., Tavernier, A., Boulet, G., Ezzahar, J., Merlin, O., Khabba, S., 2017. Performance of the two-source energy budget (TSEB) model for the monitoring of evapotranspiration over irrigated annual crops in North Africa. Agric. Water Manag. 193. https://doi.org/10.1016/j.agwat.2017.08.007.

Dick, A., Raynaud, J.L., Rolland, A., Pelou, S., Coustance, S., Dedieu, G., Hagolle, O., Burochin, J.P., Binet, R., Moreau, A., 2022. VENμS: mission characteristics, final evaluation of the first phase and data production. Remote Sens. 14, 3281. https://doi.org/10.3390/rs14143281.

Duchemin, B., Hadria, R., Erraki, S., Boulet, G., Maisongrande, P., Chehbouni, A., Escadafal, R., Ezzahar, J., Hoedjes, J.C.B., Kharrou, M.H., Khabba, S., Mougenot, B., Olioso, A., Rodriguez, J.C., Simonneaux, V., 2006. Monitoring wheat phenology and irrigation in Central Morocco: On the use of relationships between evapotranspiration, crops coefficients, leaf area index and remotely-sensed vegetation indices. Agric. Water Manag. 79, 1–27. https://doi.org/10.1016/j.agwat.2005.02.013.

Elfarkh, J., Ezzahar, J., Er-Raki, S., Simonneaux, V., Ait Hssaine, B., Rachidi, S., Brut, A., Rivalland, V., Khabba, S., Chehbouni, G., 2020. Multi-Scale evaluation of the TSEB model over a complex agricultural landscape in Morocco. Remote Sens. 12 (7), 1181. https://doi.org/10.3390/rs12071181.

Elfarkh, J., Simonneaux, V., Jarlan, L., Ezzahar, J., Boulet, G., Chakir, A., Er-Raki, S., 2022. Evapotranspiration estimates in a traditional irrigated area in semi-arid Mediterranean. Comparison of four remote sensing-based models. Agric. Water Manag. 270, 107728 https://doi.org/10.1016/j.agwat.2022.107728.

Engdahl, M.E., Borgeaud, M., Member, S., Rast, M., 2001. The Use of ERS-1/2 tandem interferometric coherence in the estimation of agricultural crop heights. IEEE Trans. Geosci. Remote Sens. 39, 1799–1806 https://doi.org/0.1109/36.942558.

Er-Raki, S., Chehbouni, A., Guemouria, N., Duchemin, B., Ezzahar, J., Hadria, R., 2007. Combining FAO-56 model and ground-based remote sensing to estimate water consumptions of wheat crops in a semi-arid region. Agric. Water Manag. 87, 41–54. https://doi.org/10.1016/j.agwat.2006.02.004.

Er-Raki, S., Chehbouni, A., Hoedjes, J., Ezzahar, J., Duchemin, B., Jacob, F., 2008. Improvement of FAO-56 method for olive orchards through sequential assimilation of thermal infrared-based estimates of ET. . Agric. Water Manag. 95, 309–321. https://doi.org/10.1016/j.agwat.2007.10.013.

Er-Raki, S., Rodriguez, J.C., Garatuza-Payan, J., Watts, C.J., Chehbouni, A., 2013. Determination of crop evapotranspiration of table grapes in a semi-arid region of Northwest Mexico using multi-spectral vegetation index. Agric. Water Manag. 122, 12–19. https://doi.org/10.1016/j.agwat.2013.02.007.

European space agency, 2012. Sentinel-1: ESA's Radar Observatory Mission for GMES Operational Services. ESA Communications, Noordwijk, The Netherlands.

Feng, P., Liu, D.L., Wang, B., Waters, C., Zhang, M., Yu, Q., 2019. Projected changes in drought across the wheat belt of southeastern Australia using a downscaled climate ensemble. Int. J. Climatol. 39, 1041–1053. https://doi.org/10.1002/joc.5861.

Filgueiras, R., Mantovani, E.C., Althoff, D., Fernandes Filho, E.I., da Cunha, F.F., 2019. Crop NDVI monitoring based on sentinel 1. Remote Sens. 11. https://doi.org/10.3390/rs11121441.

Foken, T., Wichura, B., Klemm, O., Gerchau, J., Winterhalter, M., Weidinger, T., 2001. Micrometeorological measurements during the total solar eclipse of August 11, 1999. Meteorol. Z. 10, 171–178. https://doi.org/10.1127/0941-2948/2001/0010-0171.

Foken, T.F., Wimmer, F., Mauder, M., Thomas, C., Liebethal, C., Some, C.L., 2006. Some aspects of the energy balance closure problem. Atmos. Chem. Phys. 6, 4395–4402. https://doi.org/10.5194/acp-6-4395-2006.

French, A.N., Hunsaker, D.J., Sanchez, C.A., Saber, M., Gonzalez, J.R., Anderson, R., 2020. Satellite-based NDVI crop coefficients and evapotranspiration with eddy covariance validation for multiple durum wheat fields in the US Southwest. Agric. Water Manag. 239, 106266 https://doi.org/10.1016/j.agwat.2020.106266.

Frison, P.L., Lardeux, C., 2018. Vegetation cartography from Sentinel-1 Radar Images. In: Baghdadi, N., Mallet, C., Zribi, M. (Eds.), QGIS and Applications in Agriculture and Forest. Wiley Elsevier Ltd, Oxford, UK, London, pp. 181–214. https://doi.org/10.1002/9781119457107. , UK, 2017.

Frison, P.L., Fruneau, B., Kmiha, S., Soudani, K., Dufrêne, E., Le Toan, T., Koleck, T., Villard, L., Mougin, E., Rudant, J.P., 2018. Potential of Sentinel-1 data for monitoring temperate mixed forest phenology. Remote Sens. 10, 2049. https://doi.org/10.3390/rs10122049.

Gherboudj, I., Magagi, R., Berg, A.A., Toth, B., 2011. Soil moisture retrieval over agricultural fields from multi-polarized and multi-angular RADARSAT-2 SAR data. Remote Sens. Environ. 115, 33–43. https://doi.org/10.1016/j.rse.2010.07.011.

Gibelin, A.-L., 2007. Cycle du carbone dans un modèle de surface continentale: modélisation, validation et mise en oeuvre à l'échelle globale.

Glenn, E.P., Neale, C.M.U., Hunsaker, D.J., Nagler, P.L., 2011. Vegetation index-based crop coefficients to estimate evapotranspiration by remote sensing in agricultural and natural ecosystems. Hydrol. Process. 25, 4050–4062. https://doi.org/10.1002/hyp.8392.

Gontia, N.K., Tiwari, K.N., 2010. Estimation of crop coefficient and evapotranspiration of wheat (Triticum aestivum) in an irrigation command using remote sensing and GIS. Water Resour. Manag. 24, 1399–1414. https://doi.org/10.1007/s11269-009-9505-3.

González-Dugo, M.P., Mateos, L., 2008. Spectral vegetation indices for benchmarking water productivity of irrigated cotton and sugarbeet crops. Agric. Water Manag. 95, 48–58. https://doi.org/10.1016/j.agwat.2007.09.001.

Greifeneder, F., Notarnicola, C., Hahn, S., Vreugdenhil, M., Reimer, C., Santi, E., Paloscia, S., Wagner, W., 2018. The added value of the VH/VV polarization-ratio for global soil moisture estimations from scatterometer data. IEEE J. Sel. Top. Appl. Earth Obs. Remote Sens. 11, 3668–3679. https://doi.org/10.1109/JSTARS.2018.2865185.

Hagolle, O., Huc, M., Pascual, D.V., Dedieu, G., 2015. A multi-temporal and multi-spectral method to estimate aerosol optical thickness over land, for the atmospheric correction of FormoSat-2, LandSat, VENμS and Sentinel-2 images. Remote Sens. 7, 2668–2691. https://doi.org/10.3390/rs70302668.

Hamadi, A., Albinet, C., Borderies, P., Koleck, T., Villard, L., Ho Tong Minh, D., Le Toan, T., 2014. Temporal survey of polarimetric P-Band scattering of tropical forests. IEEE Trans. Geosci. Remote Sens. 52, 4539–4547. https://doi.org/10.1109/TGRS.2013.2282357.

Howell, T.A., Steiner, J.L., Schneider, A.D., Evett, S.R., 1995. Evapotranspiration of irrigated winter wheat - Southern high plains. Trans. Am. Soc. Agric. Eng. 38, 745–759. https://doi.org/10.13031/2013.27888.

Huete, A., Didan, K., Miura, T., Rodriguez, E.P., Gao, X., Ferreira, L.G., 2002. Overview of the radiometric and biophysical performance of the MODIS vegetation indices. Inorg. Chim. Acta 83, 195–213. https://doi.org/10.1016/s0034-4257(02)00096.

Huete, A.R., 1988. A soil-adjusted vegetation index (SAVI). Remote Sens. Environ. 25, 295–309. https://doi.org/10.1016/0034-4257(88)90106-X.

Huete, A.R., Liu, H.Q., 1994. An Error and Sensitivity Analysis of the Atmospheric and Soil-Correcting Variants of the NDVI for the MODISEOS. IEEE Trans. Geosci. Remote Sens. 32, 897–905. https://doi.org/10.1109/36.298018.

Hunsaker, D.J., Pinter, P.J., Barnes, E.M., Kimball, B.A., 2003. Estimating cotton evapotranspiration crop coefficients with a multispectral vegetation index. Irrig. Sci. 22, 95–104. https://doi.org/10.1007/s00271-003-0074-6.

Hunsaker, D.J., Pinter, P.J., Kimball, B.A., 2005. Wheat basal crop coefficients determined by normalized difference vegetation index. Irrig. Sci. 24, 1–14. https://doi.org/10.1007/s00271-005-0001-0.

Ihuoma, S.O., Madramootoo, C.A., 2017. Recent advances in crop water stress detection. Comput. Electron. Agric. 141, 267–275. https://doi.org/10.1016/j.compag.2017.07.026.

IPCC, 2019. Climate Change and Land: an IPCC special report on climate change, desertification, land degradation, sustainable land management, food security, and greenhouse gas fluxes in terrestrial ecosystems.

Irmak, S., Odhiambo, L.O., Specht, J.E., Djaman, K., 2013. Hourly and daily single and basal evapotranspiration crop coefficients as a function of growing degree days, days after emergence, leaf area index, fractional green canopy cover, and plant phenology for soybean. Trans. ASABE 56, 1785–1803. https://doi.org/10.13031/trans.56.10219.

Jacome, A., Bernier, M., Chokmani, K., Gauthier, Y., Poulin, J., De Sève, D., 2013. Monitoring volumetric surface soil moisture content at the La Grande basin boreal wetland by radar multi polarization data. Remote Sens. 5, 4919–4941. https://doi.org/10.3390/rs5104919.

Jarlan, L., Khabba, S., Er-Raki, S., Le Page, M., Hanich, L., Fakir, Y., Merlin, O., Mangiarotti, S., Gascoin, S., Ezzahar, J., Kharrou, M.H., Berjamy, B., Saaïdi, A., Boudhar, A., Benkaddour, A., Laftouhi, N., Abaoui, J., Tavernier, A., Boulet, G., Simonneaux, V., Driouech, F., El Adnani, M., El Fazziki, A., Amenzou, N., Raibi, F., El Mandour, H., Ibouh, H., Le Dantec, V., Habets, F., Tramblay, Y., Mougenot, B., Leblanc, M., El Faïz, M., Drapeau, L., Coudert, B., Hagolle, O., Filali, N., Belaqziz, S., Marchane, A., Szczypta, C., Toumi, J., Diarra, A., Aouade, G., Hajhouji, Y., Nassah, H., Bigeard, G., Chirouze, J., Boukhari, K., Abourida, A., Richard, B., Fanise, P., Kasbani, M., Chakir, A., Zribi, M., Marah, H., Naimi, A., Mokssit, A., Kerr, Y., Escadafal, R., 2015. Remote Sensing of Water Resources in Semi- Arid Mediterranean Areas: the joint international laboratory TREMA. Int. J. Remote Sens. 36, 4879–4917. https://doi.org/10.1080/01431161.2015.1093198.

Jarlan, L., Albergel, C., Bonan, B., Calvet, J.C., De Rosnay, P., Ottlé, C., Peylin, P., 2021. Applications de l'assimilation de données de télédétection au suivi des surfaces continentales. In: Inverison et Assimilation de Données. ISTE-Wiley (soumis à l'éditeur en Chef), p. 44.

Kamble, B., Kilic, A., Hubbard, K., 2013. Estimating crop coefficients using remote sensing-based vegetation index. Remote Sens. 5, 1588–1602. https://doi.org/10.3390/rs5041588.

Kullberg, E.G., DeJonge, K.C., Chávez, J.L., 2016. Evaluation of thermal remote sensing indices to estimate crop evapotranspiration coefficients. Agric. Water Manag. 179, 64–73. https://doi.org/10.1016/j.agwat.2016.07.007.

Le Page, M., Toumi, J., Khabba, S., Hagolle, O., Tavernier, A., Hakim Kharrou, M., Er-Raki, S., Huc, M., Kasbani, M., Moutamanni, A., El, Yousfi, M., Jarlan, L., 2014. A life-size and near real-time test of irrigation scheduling with a sentinel-2 like time series (SPOT4-Take5) in Morocco. Remote Sens 6, 11182–11203. https://doi.org/10.3390/rs61111182.

Li, J., Wang, S., 2018. Using SAR-derived vegetation descriptors in a water cloud model to improve soil moisture retrieval. Remote Sens 10, 1370. https://doi.org/10.3390/rs10091370.

Liu, S.M., Xu, Z.W., Wang, W.Z., Jia, Z.Z., Zhu, M.J., Bai, J., Wang, J.M., 2011. A comparison of eddy-covariance and large aperture scintillometer measurements with respect to the energy balance closure problem. Hydrol. Earth Syst. Sci. 15, 1291–1306.

López-Urrea, R., Martínez-Molina, L., de la Cruz, F., Montoro, A., González-Piqueras, J., Odi-Lara, M., Sánchez, J.M., 2016. Evapotranspiration and crop coefficients of irrigated biomass sorghum for energy production. Irrig. Sci. 34, 287–296. https://doi.org/10.1007/s00271-016-0503-y.

Mattia, F., Toan, T., Le, Picard, G., Posa, F.I., Alessio, A.D., Notarnicola, C., Gatti, A.M., Rinaldi, M., Satalino, G., Le Toan, T., Picard, G., Posa, F.I., D'Alessio, A., Notarnicola, C., Gatti, A.M., Rinaldi, M., Satalino, G., Pasquariello, G., 2003. Multitemporal C-band radar measurements on wheat fields. IEEE Trans. Geosci. Remote Sens. 41, 1551–1560. https://doi.org/10.1109/TGRS.2003.813531.

Mattia, F., Balenzano, A., Rinaldi, M., Steduto, P., Moreno, J., 2015. SENTINEL-1 FOR WHEAT MAPPING AND SOIL MOISTURE RETRIEVAL, in: 2015 IEEE International Geoscience and Remote Sensing Symposium (IGARSS). pp. 2832–2835. https://doi.org/10.1109/IGARSS.2015.7326404.

MedECC, 2020. Climate and Environmental Change in the Mediterranean basin.

Mestre-Quereda, A., Lopez-Sanchez, J.M., Vicente-Guijalba, F., Jacob, A.W., Engdahl, M. E., 2020. Time-series of sentinel-1 interferometric coherence and backscatter for crop-type mapping. IEEE J. Sel. Top. Appl. Earth Obs. Remote Sens. 13, 4070–4084. https://doi.org/10.1109/JSTARS.2020.3008096.

Meyers, T.P., Hollingerb, S.E., 2004. An assessment of storage terms in the surface energy balance of maize and soybean. Agric. For. Meteorol. 125, 105–115. https://doi.org/10.1016/j.agrformet.2004.03.001.

Moeremans, B., Dautrebande, S., 2000. Soil moisture evaluation by means of multi-temporal ERS SAR PRI images and interferometric coherence. J. Hydrol. 234, 162–169. https://doi.org/10.1016/S0022-1694(00)00251-1.

Molan, Y.E., Lu, Z., 2020. Can InSAR coherence and closure phase be used to estimate soil moisture changes. Remote Sens. 12. https://doi.org/10.3390/RS12091511.

Moore, C.J., 1986. Frequency response corrections for eddy correlation systems. Boundary. Meteorol. 37, 17–35. https://doi.org/10.1016/j.agwat.2005.02.013 (Manag. 79, 1–27).

Morrison, K., Bennett, J.C., Nolan, M., Menon, R., 2011. Laboratory measurement of the DInSAR response to spatiotemporal variations in soil moisture. IEEE J. Mag. IEEE Trans. Geosci. Remote Sens 49, 3815–3823. https://doi.org/10.1109/TGRS.2011.2132137.

Norman, J.M., Kustas, W.P., Humes, K.S., 1995. Source approach for estimating soil and vegetation energy fluxes in observations of directional radiometric surface temperature. Agric. For. Meteorol. 77, 263–293. https://doi.org/10.1016/0168-1923(95)02265-Y.

Olivera-Guerra, L., Merlin, O., Er-Raki, S., Khabba, S., Escorihuela, M.J., 2018. Estimating the water budget components of irrigated crops: Combining the FAO-56 dual crop coefficient with surface temperature and vegetation index data. Agric. Water Manag. 208, 120–131. https://doi.org/10.1016/j.agwat.2018.06.014.

Ouaadi, N., Jarlan, L., Ezzahar, J., Zribi, M., Khabba, S., Bouras, E., Bousbih, S., Frison, P., 2020. Monitoring of wheat crops using the backscattering coe ffi cient and the interferometric coherence derived from Sentinel-1 in semi-arid areas. Remote Sens. Environ. 251, 112050 https://doi.org/10.1016/j.rse.2020.112050.

Ouaadi, N., Ezzahar, J., Khabba, S., Er-Raki, S., Chakir, A., Ait Hssaine, B., Le Dantec, V., Rafi, Z., Beaumont, A., Kasbani, M., Jarlan, L., 2021a. C-band radar data and in situ measurements for the monitoring of wheat crops in a semi-arid area (center of Morocco). Earth Syst. Sci. Data 13, 3707–3731. https://doi.org/10.5194/essd-13-3707-2021.

Ouaadi, N., Jarlan, L., Khabba, S., Ezzahar, J., Le Page, M., Merlin, O., 2021b. Irrigation amounts and timing retrieval through data assimilation of surface soil moisture into the FAO-56 approach in the south mediterranean region. Remote Sens. 13 (2667).

Pereira, L.S., Paredes, P., Hunsaker, D.J., López-Urrea, R., Mohammadi Shad, Z., 2021. Standard single and basal crop coefficients for field crops. Updates and advances to the FAO56 crop water requirements method. Agric. Water Manag. 243, 106466 https://doi.org/10.1016/j.agwat.2020.106466.

Pôças, I., Calera, A., Campos, I., Cunha, M., 2020. Remote sensing for estimating and mapping single and basal crop coefficientes: a review on spectral vegetation indices approaches. Agric. Water Manag. 233, 106081 https://doi.org/10.1016/j.agwat.2020.106081.

Rafi, Z., Merlin, O., Le, V., Khabba, S., Mordelet, P., Er-raki, S., Amazirh, A., Olivera-guerra, L., Ait, B., 2019. Partitioning evapotranspiration of a drip-irrigated wheat crop: inter- comparing eddy covariance-, sap fl ow-, lysimeter- and FAO-based methods. Agric. For. Meteorol. 265, 310–326. https://doi.org/10.1016/j.agrformet.2018.11.031.

Sánchez, J.M., López-Urrea, R., Doña, C., Caselles, V., González-Piqueras, J., Niclòs, R., 2015. Modeling evapotranspiration in a spring wheat from thermal radiometry: crop coefficients and E/T partitioning. Irrig. Sci. 33, 399–410. https://doi.org/10.1007/s00271-015-0476-2.

Scott, C.P., Lohman, R.B., Jordan, T.E., 2017. InSAR constraints on soil moisture evolution after the March 2015 extreme precipitation event in Chile. Sci. Rep. 7. https://doi.org/10.1038/s41598-017-05123-4.

Scott, R.W.C., Garatuza-Payan, J., Edwards, E., Goodrich, D.C., Williams, D.G., Shuttleworth, W.J., 2003. The understory and overstory partitioning of energy and water fluxes in an open canopy, semi-arid woodland. Agric. For. Meteorol. 114, 127–139.

Simonneaux, V., Hanich, L., Boulet, G., Thomas, S., 2008. Modelling runoff in the Rheraya Catchment (High Atlas, Morocco) using the simple daily model GR4J. Trends over the last decades. Materials and Methods The GR4J Model.

Simonneaux, V., Le Page, M., Helson, D., Thomas, S., 2009. Spatialized estimates of evapotranspiration of irrigated crops using remote sensing: Application to irrigation management in the Haouz plain (Marrakech, Morocco). Secheresse 20, 123–130.

Soer, G.J.R., 1980. Estimation of regional evapotranspiration and soil moisture conditions using remotely sensed crop surface temperatures. Remote Sens. Environ. 9, 27–45. https://doi.org/10.1016/0034-4257(80)90045-0.

Srivastava, P.K., O'Neill, P., Cosh, M., Lang, R., Joseph, A., 2015. Evaluation of radar vegetation indices for vegetation water content estimation using data from a ground-based SMAP simulator. Int. Geosci. Remote Sens. Symp. 2015-Novem, pp. 1296–1299. ⟨https://doi.org/10.1109/IGARSS.2015.7326012⟩.

Subedi, A., Chávez, J.L., 2015. Crop Evapotranspiration (ET) estimation models: a review and discussion of the applicability and limitations of ET Methods. J. Agric. Sci. 7, 50–68. https://doi.org/10.5539/jas.v7n6p50.

Torres, E.A., Calera, A., 2010. Evaporation du sol nu sous demande évaporatoire élevée. Une proposition de modification du modèle FAO-56. Hydrol. Sci. J. 55, 303–315. https://doi.org/10.1080/02626661003683249.

Torres, R., Snoeij, P., Geudtner, D., Bibby, D., Davidson, M., Attema, E., Potin, P., Rommen, B., Floury, N., Brown, M., Navas, I., Deghaye, P., Duesmann, B., Rosich, B., Miranda, N., Bruno, C., Abbate, M.L., Croci, R., Pietropaolo, A., Huchler, M., Rostan, F., 2012. GMES Sentinel-1 mission. Remote Sens. Environ. 120, 9–24. https://doi.org/10.1016/j.rse.2011.05.028.

Twine, T.E., Kustas, W.P., Norman, J.M., Cook, D.R., Houser, P.R., Meyers, T.P., Prueger, J.H., Starks, P.J., Wesely, M.L., 2000. Correcting eddy-covariance flux underestimates over a grassland. Agric. For. Meteorol. 103, 279–300. https://doi.org/10.1016/S0168-1923(00)00123-4.

Ulaby, F.T., Moore, R.K., Fung, A.K., 1986. Microwave remote sensing: Active and Passive, Volume III-from theory to applications.

Van Dijk, A., Moene, A.F., de Bruin, H.A.R., 2004. The principles of surface flux physics: theory, practice and description of the ECPACK library, Internal Report 2004/1, Meteorology and Air Quality Group. the Netherlands.

Veloso, A., Mermoz, S., Bouvet, A., Le Toan, T., Planells, M., Dejoux, J.F., Ceschia, E., 2017. Understanding the temporal behavior of crops using Sentinel-1 and Sentinel-2-like data for agricultural applications. Remote Sens. Environ. 199, 415–426. https://doi.org/10.1016/j.rse.2017.07.015.

Wegmuller, U., Werner, C., 1997. Retrieval of vegetation parameters with SAR interferometry. IEEE Trans. Geosci. Remote Sens. 35, 18–24. https://doi.org/10.1109/36.551930.

Wiegand, C.L., Richardson, A.J., Escobar, D.E., Gerbermann, A.H., 1991. Vegetation indices in crop assessments. Remote Sens. Environ. 35, 105–119. https://doi.org/10.1016/0034-4257(91)90004-P.

Wilson, K., Goldstein, A., Falge, E., Aubinet, M., Baldocchi, D., Berbigier, P., Bernhofer, C., Ceulemans, R., Dolman, H., Field, C., et al., 2002. Energy balance closure at FLUXNET sites. Agric. For. Meteorol. 113, 223–243.

Xiang, K., Li, Y., Horton, R., Feng, H., 2020. Similarity and difference of potential evapotranspiration and reference crop evapotranspiration – a review. Agric. Water Manag. 232, 106043 https://doi.org/10.1016/j.agwat.2020.106043.

Yao, N., Li, Y., Xu, F., Liu, J., Chen, S., Ma, H., Chau, H.W., Liu, D.L., Li, M., Feng, H., Yu, Q., He, J., 2020. Permanent wilting point plays an important role in simulating winter wheat growth under water deficit conditions. Agric. Water Manag. 229, 105954 https://doi.org/10.1016/j.agwat.2019.105954.

Zhang, G., Liu, C., Xiao, C., Xie, R., Ming, B., Hou, P., Liu, G., Xu, W., Shen, D., Wang, K., Li, S., 2017. Optimizing water use efficiency and economic return of super high yield spring maize under drip irrigation and plastic mulching in arid areas of China. Field Crop. Res 211, 137–146. https://doi.org/10.1016/j.fcr.2017.05.026.

Zhang, Y., Peña-Arancibia, J.L., McVicar, T.R., Chiew, F.H.S., Vaze, J., Liu, C., Lu, X., Zheng, H., Wang, Y., Liu, Y.Y., Miralles, D.G., Pan, M., 2016. Multi-decadal trends in global terrestrial evapotranspiration and its components. Sci. Rep. 6, 1–12. https://doi.org/10.1038/srep19124.